Research Square

Preprints are preliminary reports that have not undergone peer review.
They should not be considered conclusive, used to inform clinical practice,
or referenced by the media as validated information.

Phytochemical profiling, multi-target enzyme inhibition, and cytotoxicity assessment of Galium dumosum Boiss.: an integrated in vitro and in silico study

İlhan Sabancilar

isabancilar@beu.edu.tr

Bitlis Eren University

Abdülmelik Aras

Iğdır University

Alpaslan Bayrakdar

Iğdır University

Ercan Oğuz

Iğdır University

Fikret Türkan

Iğdır University

Ömer Kılıç

Adıyaman University

Mustafa Yaşar

Muş Alparslan University

Mehmet Doğru

Dicle University

Article

Keywords: Galium dumosum, LC–MS/MS, phenolic compounds, antioxidant activity, enzyme inhibition, molecular dynamics simulations

Posted Date: November 25th, 2026

DOI: https://doi.org/10.21203/rs.3.rs-11694525/v1

License: This work is licensed under a Creative Commons Attribution 4.0 International License.
Read Full License

Additional Declarations: No competing interests reported.

Phytochemical profiling, multi-target enzyme inhibition, and cytotoxicity assessment of *Galium dumosum* Boiss.: an integrated *in vitro* and *in silico* study

İlhan Sabancilar[1*], Abdülmelik Aras[2,7], Alpaslan Bayrakdar[3], Ercan Oğuz[3], Fikret Türkan[4], Ömer Kılıç[5], Mustafa Yaşar[2], Mehmet Doğru[6]

[1]Department of Medical Services and Techniques, Vocational School of Health Services, Bitlis Eren University, 13000 Bitlis, Türkiye

[2]Department of Plant Production and Technologies, Faculty of Applied Sciences, Muş Alparslan University, 49250 Muş, Türkiye

[3]Department of Medical Services and Techniques, Vocational School of Health Services, Iğdır University, 76000 Iğdır, Türkiye

[4]Department of Basic Sciences, Faculty of Dentistry, Iğdır University, 76000 Iğdır, Türkiye

[5]Department of Pharmaceutical Sciences, Faculty of Pharmacy, Adıyaman University, 02040 Adıyaman, Türkiye

[6]Department of Chemistry, Faculty of Science, Dicle University, 21280 Diyarbakır, Türkiye

[7]Department of Biochemistry, Faculty of Science and Arts, Iğdır University, Iğdır, Türkiye

*Corresponding author: İlhan Sabancilar (e-mail: isabancilar@beu.edu.tr)

Abstract

Galium dumosum Boiss. is a perennial species endemic to Türkiye whose chemistry and bioactivity have received little attention. Methanol (MeOH) and dichloromethane (DCM) extracts of its aerial parts were profiled by LC–MS/MS and tested for antioxidant capacity, inhibition of acetylcholinesterase (AChE), α-glucosidase, and α-amylase, and cytotoxicity; five quantified phenolics were further examined by docking, molecular dynamics, and MM/GBSA calculations. Eleven phenolics were quantified in the MeOH extract, led by vanillin (17.917 µg/g), chlorogenic acid (8.527 µg/g), and trans-cinnamic acid (5.133 µg/g), whereas vanillin dominated the DCM extract (48.939 µg/g). The MeOH extract was the more active of the two, with an $ABTS^{\bullet+}$ IC_{50} of 15.7 ± 2.1 µg/mL and IC_{50} values of 1.095, 1.050, and 1.070 µg/mL against AChE, α-glucosidase, and α-amylase. It did not reduce MIA PaCa-2 or HUVEC viability to 50% at concentrations up to 1000 µg/mL. Rutin gave the most favorable docking scores against the three enzymes (−10.46, −9.04, and −9.32 kcal/mol) and remained bound throughout 50-ns simulations, with MM/GBSA energies of −32.61, −16.20, and −29.80

kcal/mol. Rutin and the phenolic acids are therefore likely contributors to the enzyme inhibition, whereas the data do not support a direct anticancer effect.

Keywords: *Galium dumosum*, LC–MS/MS, phenolic compounds, antioxidant activity, enzyme inhibition, molecular dynamics simulations

Introduction

Medicinal plants have long been used in traditional medicine and remain important sources of bioactive compounds with potential pharmaceutical applications. Their biological activities stem largely from secondary metabolites such as phenolic acids, flavonoids, terpenoids, and sterols.[1,2] The genus *Galium* L. (Rubiaceae) comprises numerous herbaceous and woody species distributed worldwide and is particularly diverse in Türkiye. More than 125 *Galium* taxa have been reported from Türkiye, with an estimated endemism rate of approximately 54%.[3] Species of *Galium* have traditionally been used for the treatment of various disorders and have been reported to exhibit antioxidant, antimicrobial, anti-inflammatory, antipyretic, hypotensive, sedative, and wound-healing properties.[4,5] Phytochemical studies of *Galium* species have reported phenolic acids, flavonoids, iridoids, anthraquinones, triterpenes, and phytosterols, which may account for these properties.[2,6]

Galium dumosum Boiss. is a perennial species endemic to Türkiye. It is characterized by a woody rootstock, numerous suberect to pendulous stems, lanceolate to narrowly elliptic leaves arranged in whorls, and hairy inflorescences.[7] Although the genus has attracted considerable phytochemical and pharmacological interest, little is known about the biological properties of *G. dumosum*. Characterizing this endemic species can therefore add to what is known of the chemical diversity of the genus and indicate whether the plant merits further medicinal investigation.

Alzheimer's disease (AD) and type 2 diabetes mellitus (T2DM) are among the most prevalent chronic disorders worldwide, and accumulating evidence indicates that they share common pathophysiological features, including insulin resistance, oxidative stress, and chronic inflammation, to the extent that AD has been described as "type 3 diabetes".[8] Inhibition of acetylcholinesterase (AChE), which hydrolyzes the neurotransmitter acetylcholine in the synaptic cleft, remains a principal symptomatic strategy in AD, and AChE inhibitors such as donepezil are among the few approved drugs for the disease.[9] In T2DM, inhibition of the carbohydrate-hydrolyzing enzymes α-amylase and α-glucosidase delays the digestion of dietary starch and oligosaccharides and thereby attenuates postprandial hyperglycemia. Clinically used

inhibitors such as acarbose, however, frequently cause gastrointestinal side effects, which has prompted the search for plant-derived alternatives.[10,11] Natural products that act on both cholinergic and carbohydrate-hydrolyzing targets are therefore of particular interest.

Phenolic compounds are among the most extensively studied natural inhibitors of these enzymes. Rutin, *p*-coumaric acid, and vanillin have been reported to inhibit pancreatic α-amylase and α-glucosidase *in vitro*, and the inhibition constants of p-coumaric acid and vanillin against α-amylase were comparable to that of acarbose.[12] p-Coumaric acid was shown to inhibit α-amylase competitively through non-covalent interactions,[13] vanillin inhibits α-glucosidase by a mixed-type mechanism,[14] and trans-cinnamic acid and its derivatives have been identified as α-glucosidase inhibitors in structure–activity relationship studies.[15] In contrast, hydroxybenzoic acids such as salicylic acid have been reported to show little inhibitory activity against carbohydrate-hydrolyzing enzymes,[11] and comparatively few studies have addressed the interactions of these small phenolics with AChE at the molecular level. Plant extracts are also complex mixtures, so the contribution of individual constituents to the overall enzyme-inhibitory activity cannot be resolved by *in vitro* assays alone.

Computational approaches offer a cost-effective means of addressing this limitation. Drug-likeness and ADMET (absorption, distribution, metabolism, excretion, and toxicity) predictions allow the pharmacokinetic suitability and potential toxicity of candidate molecules to be assessed at an early stage.[16,17] Molecular docking predicts the preferred binding pose and affinity of a ligand within the active site of a target enzyme, whereas molecular dynamics (MD) simulations evaluate the stability of the resulting complexes over time under near-physiological conditions through descriptors such as root-mean-square deviation (RMSD), root-mean-square fluctuation (RMSF), radius of gyration (Rg), and hydrogen-bond occupancy.[18] Binding free energies estimated by the molecular mechanics/generalized Born surface area (MM/GBSA) method further refine docking-based affinity rankings.[19] Integrated *in vitro* and *in silico* strategies of this kind have been successfully applied to plant extracts to identify constituents potentially responsible for enzyme inhibition.[20,21]

Testing the extracts for cytotoxicity widens their biological assessment and gives a first indication of cellular safety. The human pancreatic carcinoma cell line MIA PaCa-2 (ATCC CRL-1420) is a suitable *in vitro* model for examining the effects of plant extracts on pancreatic cancer cells. In parallel, human umbilical vein endothelial cells (HUVECs) can serve as a non-tumor cellular model to assess potential adverse effects on normal endothelial cells.[22] Assessing cell viability in both models can provide complementary information about the cellular effects

of the extracts, but such *in vitro* findings alone cannot determine anticancer efficacy or tumor selectivity.[23]

In the present study, methanol and dichloromethane extracts of the aerial parts of *G. dumosum* were analyzed for their phenolic composition by LC–MS/MS and tested for antioxidant activity, inhibition of AChE, α-glucosidase, and α-amylase, and cytotoxicity towards MIA PaCa-2 cells and HUVECs. The quantified phenolics were then examined by ADMET prediction, molecular docking, MD simulations, and MM/GBSA calculations to identify the constituents most likely to account for the enzyme inhibition. To our knowledge, this is the first report on the phytochemistry and bioactivity of *G. dumosum*.

Results and discussion

LC–MS/MS phenolic profile of *G. dumosum* extracts

The phenolic composition of the methanol (MeOH) and dichloromethane (DCM) extracts of *G. dumosum* was investigated by LC–MS/MS using multiple reaction monitoring (MRM). Twelve phenolic and related phytochemicals were quantified in at least one of the extracts: 11 in the MeOH extract and four in the DCM extract. Vanillin, protocatechuic acid, and naringenin occurred in both extracts, indicating that they partition into solvents of markedly different polarity.

The MeOH extract exhibited a considerably broader phytochemical profile than the DCM extract. Chlorogenic acid (8.527 µg/g), rutin (3.486 µg/g), p-coumaric acid (3.480 µg/g), vanillin (17.917 µg/g), trans-ferulic acid (4.436 µg/g), salicylic acid (3.129 µg/g), protocatechuic acid (1.934 µg/g), trans-cinnamic acid (5.133 µg/g), naringenin (1.663 µg/g), quercetin (2.288 µg/g), and morin (2.083 µg/g) were detected in this extract. Vanillin was the predominant compound, followed by chlorogenic acid and trans-cinnamic acid.

The DCM extract displayed a more restricted profile, with hydroxybenzaldehyde (0.349 µg/g), vanillin (48.939 µg/g), protocatechuic acid (3.144 µg/g), and naringenin (1.773 µg/g) being detected. Vanillin was by far the major compound in the DCM extract. Although the number of detected compounds was substantially lower in DCM than in MeOH, the total concentration of the quantified compounds was comparable between the two extracts (54.205 µg/g in DCM and 54.076 µg/g in MeOH). The similar totals therefore conceal very different compositions: the DCM profile was dominated by a single phenolic aldehyde, whereas the MeOH extract contained a broad range of phenolic acids and flavonoids.

The pronounced predominance of vanillin in the DCM extract may be related to differences in solvent polarity and the physicochemical characteristics of individual metabolites. Dichloromethane preferentially extracts relatively less polar constituents, whereas methanol is more effective for the extraction of polar and moderately polar phenolic compounds. The detection of chlorogenic acid, rutin, p-coumaric acid, trans-ferulic acid, salicylic acid, quercetin, and morin exclusively in the MeOH extract is consistent with this polarity-dependent extraction behavior. Conversely, the markedly higher concentration of vanillin in DCM (48.939 µg/g) than in MeOH (17.917 µg/g) suggests that vanillin has a substantial affinity for the less polar extraction environment.

Among the phenolic acids, chlorogenic acid was the most abundant compound in the MeOH extract (8.527 µg/g), followed by trans-cinnamic acid (5.133 µg/g) and trans-ferulic acid (4.436 µg/g). p-Coumaric acid (3.480 µg/g) and salicylic acid (3.129 µg/g) were also detected at appreciable levels. Protocatechuic acid was found in both extracts, with concentrations of 3.144 µg/g in DCM and 1.934 µg/g in MeOH. *G. dumosum* contains a diverse group of hydroxycinnamic- and hydroxybenzoic-acid derivatives, although their relative abundance is strongly influenced by the extraction solvent.

Flavonoids were represented primarily by rutin, naringenin, quercetin, and morin. Rutin was detected only in the MeOH extract at 3.486 µg/g, while quercetin and morin were quantified at 2.288 and 2.083 µg/g, respectively. Naringenin was the only flavonoid detected in both extracts, with comparable concentrations in DCM (1.773 µg/g) and MeOH (1.663 µg/g).

The relatively high abundance of vanillin, chlorogenic acid, trans-cinnamic acid, and several flavonoids may contribute to the biological activities observed for the extracts. The distinct chemical profiles of the MeOH and DCM extracts may also explain part of the difference in their biological activity.

The LC–MS/MS results show clear solvent-dependent differences in the chemical composition of *G. dumosum* extracts. The MeOH extract showed greater phenolic diversity and contained a broader spectrum of phenolic acids and flavonoids, whereas the DCM extract was characterized by a highly selective accumulation of vanillin together with smaller amounts of protocatechuic acid, naringenin, and hydroxybenzaldehyde. A closely comparable solvent-dependent partitioning, in which vanillin and trans-cinnamic acid accumulated preferentially in the dichloromethane fraction while chlorogenic acid and the more polar phenolic acids and flavonoids were confined to the methanol fraction, has been reported for the endemic

Asteraceae species *Gundelia komagenensis* Fırat analysed under the same extraction and LC–MS/MS conditions.[20]

Table 1. MRM parameters and quantitative LC–MS/MS results of the analyzed compounds in *G. dumosum* extracts

Compound	RT (min)	DCM extract (µg/g)	MeOH extract (µg/g)	Precursor → product ion (m/z)	Polarity	Dwell (ms)	Fragmentor (V)	CE (V)
Chlorogenic acid	2.813	0	8.527	353 → 191	−	9	110	12
Rutin	3.875	0	3.486	609.1 → 300.2	−	9	185	40
Hydroxybenzaldehyde	4.811	0.349	0	121 → 92	−	9	110	24
p-Coumaric acid	5.022	0	3.480	163.1 → 119.2	−	9	85	12
Vanillin	5.392	48.939	17.917	152.9 → 124.9; 152.9 → 93.1; 152.9 → 65.2	+	9	65	13
trans-Ferulic acid	5.602	0	4.436	195.1 → 176.9; 195.1 → 144.7; 193.1 → 133.9	+/−	9	75/95	10/14
Salicylic acid	7.597	0	3.129	137 → 93.1	−	38	85	18
Protocatechuic acid	8.448	3.144	1.934	154.9 → 136.4; 154.9 → 111; 154.9 → 93.1; 152.9 → 108.9	+/−	38	118/150	11/14
trans-Cinnamic acid	11.063	0	5.133	149.1 → 131.1; 149 → 131.1; 149 → 103; 147.1 → 103.1	+/−	18	90/75/70	6/6/10
Naringenin	11.616	1.773	1.663	270.9 → 150.8; 270.9 → 119.1	−	18	130/115	26/24
Quercetin	11.933	0	2.288	302.8 → 152.9; 302.8 → 136.9; 300.8 → 179; 300.7 → 150.9	+/−	18	125/130	34/20–22
Morin	12.026	0	2.083	302.9 → 136.8; 302.8 → 153	+	18	145	32/30

Abbreviations: MRM, multiple reaction monitoring; RT, retention time; DCM, dichloromethane; MeOH, methanol; CE, collision energy.

Note: The following compounds were not detected in either of the two plant extracts: gallic acid, epigallocatechin, catechin, gentisic acid, caffeic acid, vanillic acid, syringic acid, polydatin, isoquercitrin, taxifolin, baicalin, protocatechuic acid ethyl ester, kaempferol, resveratrol, 7-hydroxyflavone, chrysin, luteolin, biochanin A, 5-hydroxyflavone, and diosgenin. Zero values indicate that the compound was not quantified above the method reporting limit in the respective extract.

Enzyme inhibitory and antioxidant activities

Enzyme inhibitory activities

The enzyme inhibitory activities of the methanol (MeOH) and dichloromethane (DCM) extracts of *G. dumosum* were evaluated against acetylcholinesterase (AChE), α-glucosidase, and α-amylase, and the results are presented in Table 2. Both extracts exhibited pronounced inhibitory activity against all three enzymes, with IC_{50} values ranging from 1.050 to 1.434 µg/mL, and the MeOH extract was slightly more active than the DCM extract against each enzyme. The MeOH extract inhibited AChE with an IC_{50} of 1.095 ± 0.515 µg/mL, whereas the DCM extract showed an IC_{50} value of 1.190 ± 0.145 µg/mL. The lower IC_{50} value of the MeOH extract indicates. Although the difference between the two extracts was relatively small, the slightly stronger activity of the MeOH extract may be associated with its greater ability to solubilize and extract polar and moderately polar secondary metabolites capable of interacting with AChE.

Both extracts also showed strong inhibitory activity against carbohydrate-hydrolyzing enzymes. The MeOH extract exhibited an IC_{50} value of 1.050 ± 0.158 µg/mL against α-glucosidase, while the corresponding value for the DCM extract was 1.434 ± 1.098 µg/mL. Compared with acarbose (IC_{50} = 1.497 ± 0.245 µg/mL), both extracts showed lower IC_{50} values, indicating stronger inhibitory activity under the present assay conditions. The MeOH extract was particularly active. A similar trend was observed for α-amylase, for which the MeOH and DCM extracts exhibited IC_{50} values of 1.070 ± 0.258 and 1.380 ± 0.925 µg/mL, respectively, compared with 1.497 ± 0.245 µg/mL for acarbose (Table 2).

Both extracts therefore contain constituents that inhibit these three enzymes effectively *in vitro*. The stronger activity of the MeOH extract across all three enzymes further suggests that the compounds responsible for the observed activity may be enriched in the more polar fraction.

The coefficient of determination values (R^2 = 0.9743–0.9923) indicate a high degree of goodness-of-fit for the concentration–response relationships, supporting the reliability of the calculated IC_{50} values. Even so, enzyme inhibition *in vitro* cannot be equated with therapeutic efficacy. Further studies involving enzyme kinetic analyses, identification of the active constituents, and molecular-level investigations would be required to clarify the mechanisms responsible for the observed inhibitory effects.

In summary *G. dumosum*, and particularly its MeOH extract, inhibits AChE, α-glucosidase, and α-amylase *in vitro*. The IC_{50} values obtained here (1.050–1.434 µg/mL) fall within the same narrow range as those reported for the methanol and dichloromethane extracts of *G.*

komagenensis against the same three enzymes (1.132–1.838 µg/mL) under an identical assay protocol, which indicates that comparable inhibitory potencies are attainable across taxonomically unrelated endemic species.[20] Because the same extract acts on both cholinergic and carbohydrate-hydrolyzing targets, the plant merits further study as a source of metabolites relevant to neurodegenerative and metabolic disorders.

Table 2. Antioxidant and enzyme inhibitory activities of *G. dumosum* extracts and reference standards

Sample	AChE IC_{50} (µg/mL)	R^2	α-Glucosidase IC_{50} (µg/mL)	R^2	α-Amylase IC_{50} (µg/mL)	R^2	$ABTS^{\bullet+}$ IC_{50} (µg/mL)	SD	FRAP reducing power*
G. dumosum MeOH	1.095 ± 0.515	0.9923	1.050 ± 0.158	0.9758	1.070 ± 0.258	0.9918	15.7	2.107	4th
G. dumosum DCM	1.190 ± 0.145	0.9743	1.434 ± 1.098	0.9848	1.380 ± 0.925	0.9852	19.8	1.639	5th
BHA	–	–	–	–	–	–	11.4	3.728	2nd
BHT	–	–	–	–	–	–	12.6	3.458	3rd
Ascorbic acid (AA)	–	–	–	–	–	–	13.4	5.043	1st

Note: Values are expressed as mean ± standard deviation (SD). Lower IC_{50} values indicate stronger inhibitory or radical-scavenging activity. FRAP reducing power at 50 µg/mL was ranked as AA > BHA > BHT > *G. dumosum* MeOH > *G. dumosum* DCM. AChE, acetylcholinesterase; DCM, dichloromethane; MeOH, methanol; BHA, butylated hydroxyanisole; BHT, butylated hydroxytoluene; AA, ascorbic acid; R^2, coefficient of determination. *FRAP ranking represents relative reducing capacity at 50 µg/mL.

Antioxidant activities

The antioxidant potential of *G. dumosum* extracts was evaluated using the ABTS radical-scavenging and ferric reducing antioxidant power (FRAP) assays. The results are summarized in **Table 2**. In the ABTS assay, the MeOH extract exhibited an IC_{50} value of 15.7 ± 2.1 µg/mL, whereas the DCM extract showed an IC_{50} value of 19.8 ± 1.6 µg/mL. Because a lower IC_{50} indicates stronger scavenging, the MeOH extract was the more effective of the two.

The activity of the MeOH extract was relatively close to that of the reference antioxidants. The IC_{50} values obtained for BHA, BHT, and ascorbic acid (AA) were 11.4 ± 3.7, 12.6 ± 3.5, and 13.4 ± 5.0 µg/mL, respectively. All three standards were therefore more active than the extracts, BHA giving the lowest IC_{50}, although both extracts still showed appreciable radical-scavenging activity.

The stronger activity of the MeOH extract compared with the DCM extract may be related to differences in the polarity and composition of the extracted phytochemicals. Methanol is

generally more effective in extracting a broad range of polar and moderately polar phenolic compounds, flavonoids, and other antioxidant constituents. The higher $ABTS^{\bullet+}$ scavenging activity of the MeOH extract may reflect a greater abundance or more favorable combination of radical-scavenging constituents in this fraction. However, because the extracts contain complex mixtures of compounds, the antioxidant activity cannot be attributed to a single compound without further phytochemical characterization.

The FRAP assay provided a complementary assessment of the reducing capacity of the extracts. At a concentration of 50 µg/mL, the ferric ion (Fe^{3+})-reducing capacities followed the order Ascorbic acid > BHA > BHT > *G. dumosum* MeOH > *G. dumosum* DCM. Ascorbic acid showed the highest reducing capacity among the tested samples, whereas the DCM extract showed the lowest reducing capacity. The MeOH extract again performed better than the DCM extract, consistent with the trend observed in the ABTS assay.

In both assays, *G. dumosum* showed appreciable antioxidant capacity, and the MeOH extract was consistently more active than the DCM extract. The $ABTS^{\bullet+}$ IC_{50} values recorded here (15.7–19.8 µg/mL) are of the same order as those reported for extracts of *G. komagenensis* (13.7–14.5 µg/mL).

Cytotoxic activity and selectivity

The cytotoxic effects of the methanolic extract of *G. dumosum were* evaluated against MIA PaCa-2 pancreatic cancer cells and non-tumorigenic HUVECs using the MTT assay after 24 and 48 h of exposure. The extract did not induce a significant reduction in cell viability in either cell line within the tested concentration range, suggesting limited cytotoxic activity under the experimental conditions. In MIA PaCa-2 cells, the calculated IC_{50} values were 1854 µg/mL at 24 h and 1015 µg/mL at 48 h. However, both values exceeded the highest concentration tested, and the low coefficients of determination indicate a poor regression fit, so these estimates are not reliable measures of cytotoxic potential. The apparent decrease in IC_{50} at 48 h should therefore not be interpreted as evidence of increased cytotoxic activity with prolonged exposure. IC_{50} estimates of this kind need to be read together with the concentration–response curves and the quality of the regression, particularly in colorimetric cytotoxicity assays.[23,24]

The absence of a consistent concentration-dependent response in either cell line also prevented the determination of a meaningful selectivity index. Although LC–MS/MS analysis revealed several phenolic compounds in the methanolic extract, including vanillin, chlorogenic acid, trans-cinnamic acid, and rutin, the observed phytochemical composition and enzyme inhibitory

activity were not accompanied by appreciable cytotoxic effects in the tested cellular models. The biological potential of *G. dumosum* therefore appears to lie in its antioxidant and enzyme-inhibitory properties rather than in direct cytotoxicity, at least under the conditions investigated. At the same time, the lack of detectable cytotoxicity in HUVECs should not be considered sufficient evidence of general safety. The inactivity of the methanol extract does not, however, exclude cytotoxic activity in the less polar fraction. For *G. komagenensis,* the methanol extract was likewise inactive against both MIA PaCa-2 cells and HUVECs, whereas the dichloromethane extract reduced MIA PaCa-2 viability in a concentration-dependent manner while leaving HUVEC viability above 88% at every concentration and time point tested.[20] Extracts of other endemic Asteraceae taxa have shown similarly pronounced, cell-line-dependent cytotoxicity, with *Anthemis fumariifolia* Boiss. reducing the viability of MCF-7 breast and HT-29 colon carcinoma cells markedly more than that of HUVECs.[25] Further studies using complementary viability assays, additional cancer cell lines, and tissue-matched non-malignant cells are warranted to clarify the cellular effects of the extract and determine whether its biological activities have broader therapeutic relevance.

In silico analyses

Drug-likeness and ADMET properties

The drug-likeness of the five phenolic constituents was evaluated according to Lipinski's rule of five, which defines a drug-like compound as having a molecular weight (MW) ≤ 500 g/mol, a LogP ≤ 5, no more than 10 hydrogen-bond acceptors (HBA), and no more than 5 hydrogen-bond donors (HBD), with no more than one violation of these criteria being tolerated.[16] The results are summarized in **Table 3**. p-Coumaric acid, vanillin, salicylic acid, and trans-cinnamic acid complied with all four criteria, with molecular weights of 138.12–164.16 g/mol, LogP values of 1.09–1.78, and low numbers of hydrogen-bond donors (1–2) and acceptors (1–3). These small, moderately lipophilic phenolics therefore have physicochemical profiles compatible with good oral absorption. In contrast, rutin violated three of the four criteria (MW = 610.52 g/mol; 10 hydrogen-bond donors; 16 hydrogen-bond acceptors), largely because of its rutinoside (rhamnose–glucose) moiety, and its negative LogP value (−1.69) reflects its high polarity. Among the reference drugs included for comparison, donepezil satisfied all criteria, whereas acarbose also showed three violations (MW = 645.61 g/mol; 14 donors; 19 acceptors) together with a markedly negative LogP (−8.56).

Table 3. Drug-likeness properties of the phenolic constituents of *G. dumosum* and the reference drugs according to Lipinski's rule of five

Compound	MW (g/mol)	LogP	HBA	HBD	Violations	Drug-likeness
Rutin	610.52	−1.69	16	10	3 (MW, HBA, HBD)	No
p-Coumaric acid	164.16	1.49	2	2	0	Yes
Vanillin	152.15	1.21	3	1	0	Yes
Salicylic acid	138.12	1.09	2	2	0	Yes
trans-Cinnamic acid	148.16	1.78	1	1	0	Yes
Donepezil (ref.)	379.50	4.36	4	0	0	Yes
Acarbose (ref.)	645.61	−8.56	19	14	3 (MW, HBA, HBD)	No

The rule of five is, however, an empirical filter for estimating the likelihood of passive oral absorption; it is neither a measure of biological activity nor a prerequisite for therapeutic use. Lipinski and co-workers themselves noted that compound classes recognized by biological transporters, such as antibiotics, antifungals, vitamins, and cardiac glycosides, are exceptions to the rule,[16] and a considerable number of approved oral drugs, many of them derived from natural products, lie beyond the rule-of-five chemical space.[26] Acarbose, the reference α-glucosidase and α-amylase inhibitor used in this study, clearly illustrates this point: despite three violations, it is an approved antidiabetic drug with well-established efficacy. Less than 2% of an oral dose of acarbose is absorbed as active drug, and its pharmacological action is exerted locally within the gastrointestinal tract, where its target enzymes are located.[27] By analogy, the predicted poor oral absorption of rutin does not preclude inhibition of α-glucosidase and α-amylase, which act in the intestinal lumen and brush border. The drug-likeness results should therefore be regarded as a preliminary indicator and interpreted together with the docking, MD, and experimental data.

The predicted ADMET properties of the compounds are summarized in Table 4. All five compounds were predicted to be water-soluble (log S = −1.47 to −2.89 log mol/L). According to the pkCSM interpretation criteria, a compound is considered to have high Caco-2 permeability when its log Papp value exceeds 0.90, and to be poorly absorbed when its predicted human intestinal absorption is below 30%.[28] On this basis, the four small phenolics exhibited high Caco-2 permeability (log Papp = 1.14–1.49) and high intestinal absorption (77.7–94.0%), consistent with their full compliance with Lipinski's rule. Rutin, by contrast, showed low Caco-2 permeability (log Papp = −1.30) and an intestinal absorption of 27.6%, below the 30% threshold for poor absorption, and was predicted to be a P-glycoprotein (P-gp) substrate, which may further limit its net absorption. These predictions agree with experimental

evidence that rutin is poorly absorbed in its glycosidic form and is largely hydrolyzed by the colonic microbiota to its aglycone, quercetin, before absorption.[29] p-Coumaric acid was also predicted to be a P-gp substrate; however, its high predicted intestinal absorption suggests that efflux would have only a limited effect on its bioavailability.

Table 4. Predicted ADMET properties of the phenolic constituents of *G. dumosum* (pkCSM)

Parameter	Rutin	p-Coumaric acid	Vanillin	Salicylic acid	trans-Cinnamic acid
Absorption					
Water solubility (log mol/L)	−2.891	−1.610	−1.840	−1.474	−1.620
Caco-2 permeability (log Papp, 10^{-6} cm/s)	−1.296	1.142	1.196	1.144	1.491
Human intestinal absorption (%)	27.63	93.18	89.87	77.71	94.02
P-gp substrate	Yes	Yes	No	No	No
Distribution					
VDss, human (log L/kg)	0.027	−0.602	0.149	−0.750	−0.581
BBB permeability (log BB)	−2.107	−0.234	−0.237	−0.333	0.211
CNS permeability (log PS)	−5.760	−2.379	−2.272	−3.243	−1.341
Metabolism					
CYP2D6 / CYP3A4 substrate	No / No	No / No	No / No	No / No	No / No
CYP inhibition (1A2, 2C19, 2C9, 2D6, 3A4)	None	None	CYP1A2	None	None
Excretion					
Total clearance (log mL/min/kg)	−0.260	0.696	0.635	0.655	0.801
Renal OCT2 substrate	No	No	No	No	No
Toxicity					
AMES toxicity	Yes	No	No	No	No
hERG I / hERG II inhibitor	No / Yes	No / No	No / No	No / No	No / No
Hepatotoxicity	No	No	No	No	No
Skin sensitization	No	No	No	No	Yes
Oral rat acute toxicity, LD_{50} (mol/kg)	2.434	2.099	1.990	2.063	2.179

With regard to distribution, the steady-state volume of distribution (VDss) is considered low when log VDss is below −0.15 and high when it exceeds 0.45 log L/kg.[28] Rutin and vanillin showed moderate VDss values (0.027 and 0.149 log L/kg, respectively), whereas p-coumaric, salicylic, and trans-cinnamic acids had low values (−0.58 to −0.75 log L/kg), indicating that

they would be distributed mainly in plasma, consistent with their acidic character. Blood–brain barrier (BBB) and central nervous system (CNS) permeability are particularly relevant to AChE inhibition. In pkCSM, compounds with log BB > 0.3 are considered to cross the BBB readily and those with log BB < −1 to be poorly distributed to the brain, whereas compounds with log PS > −2 are considered to penetrate the CNS and those with log PS < −3 to be unable to do so.[28] Rutin was predicted to be unable to cross the BBB (log BB = −2.11) or to penetrate the CNS (log PS = −5.76). Among the small phenolics, trans-cinnamic acid displayed the most favorable profile (log BB = 0.21; log PS = −1.34) and was the only compound predicted to penetrate the CNS (log PS > −2). p-Coumaric acid and vanillin showed intermediate CNS permeability (log PS = −2.38 and −2.27, respectively), whereas salicylic acid was predicted not to penetrate (log PS = −3.24). These results suggest that any central anticholinesterase effect in vivo would more likely be associated with the small phenolics, particularly trans-cinnamic acid, than with rutin.

None of the compounds was predicted to be a substrate of the cytochrome P450 (CYP) isoforms CYP2D6 or CYP3A4, and among the five isoforms evaluated (CYP1A2, CYP2C19, CYP2C9, CYP2D6, and CYP3A4), only vanillin was predicted to inhibit one (CYP1A2), indicating a low overall potential for metabolism-based drug–drug interactions. The total clearance values of the small phenolics (0.64–0.80 log mL/min/kg) were higher than that of rutin (−0.26 log mL/min/kg), suggesting slower elimination of the larger glycoside. None of the compounds was predicted to be a substrate of the renal organic cation transporter 2 (OCT2).

In the toxicity predictions, none of the compounds was predicted to be hepatotoxic or to inhibit the human ether-à-go-go-related gene (hERG) I potassium channel, and the four small phenolics were negative in the AMES mutagenicity test. Rutin was predicted to be AMES-positive and a hERG II inhibitor. The AMES alert is probably associated with its quercetin aglycone, which is mutagenic in some bacterial assays but has shown no evidence of genotoxic or carcinogenic activity in vivo.[30] Given the low predicted absorption of rutin, its systemic exposure, and thus any hERG-related cardiac risk, would be expected to be limited. trans-Cinnamic acid was predicted to be a skin sensitizer, a finding relevant mainly to topical exposure. The predicted oral rat acute toxicity values (LD_{50} = 1.99–2.43 mol/kg) were similar across the compounds, with none standing out as acutely toxic.

The four small phenolic constituents displayed favorable predicted pharmacokinetic and safety profiles, whereas the profile of rutin indicates limited systemic availability, which is compatible with a local action on carbohydrate-hydrolyzing enzymes in the gastrointestinal tract, as in the

case of acarbose. Like the drug-likeness results, these ADMET data are computational estimates and require experimental confirmation.

Molecular docking

Molecular docking is a structure-based computational approach that predicts the preferred orientation and conformation of a ligand within the binding site of a target macromolecule and estimates the strength of the resulting interaction by means of a scoring function.[31,32] It is widely used to rationalize experimentally observed enzyme inhibition at the molecular level and to identify the key residues involved in ligand recognition. In the present study, the docking protocol was established in accordance with the procedures applied in our previous studies,[20,33] and its reliability was first assessed by re-docking the co-crystallized ligand of each enzyme structure into its binding site.

The re-docked poses reproduced the crystallographic binding modes with RMSD values of 0.38 Å for donepezil in AChE, 2.04 Å for acarbose in α-glucosidase, and 1.18 Å for the acarbose-derived oligosaccharide in α-amylase **(Figure 1)**. The donepezil and α-amylase complexes were therefore reproduced well within the generally accepted threshold of 2.0 Å. For acarbose in α-glucosidase, the acarviosine moiety occupying the catalytic subsites was reproduced with an RMSD of 0.45 Å, and the slightly higher overall value arose almost entirely from the two terminal glucose units (2.58 and 2.97 Å), which also displayed the highest crystallographic B-factors in the structure (45–56 Å² vs 26 Å² for acarviosine), reflecting their intrinsic flexibility. These results confirmed that the protocol was able to reproduce the experimentally determined binding modes and was suitable for docking the phenolic constituents.

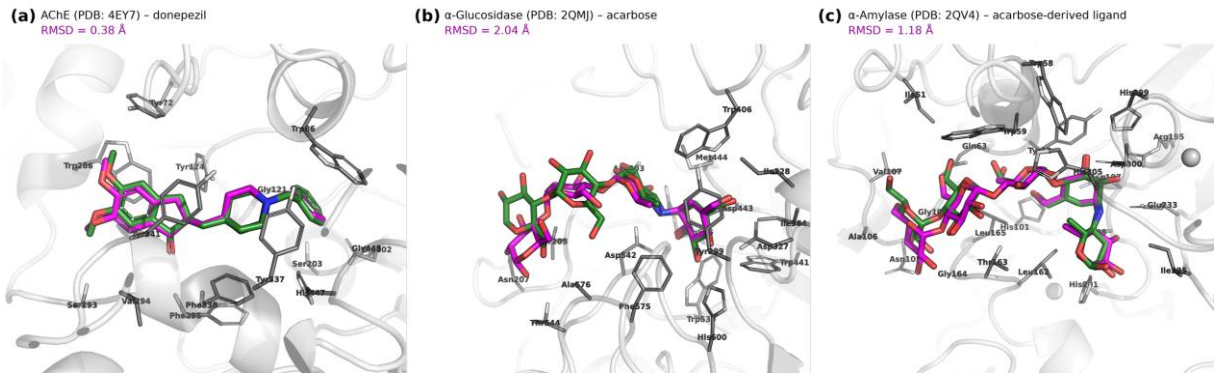

***Figure* 1**. Validation of the docking protocol by re-docking of the co-crystallized ligands. Superposition of the crystallographic (green) and top-ranked re-docked (magenta) poses: (a) donepezil in AChE (4EY7), (b) acarbose in α-glucosidase (2QMJ), (c) the acarbose-derived oligosaccharide in α-amylase (2QV4)

The binding energies, ligand efficiencies, and interactions of the five phenolic constituents and the reference inhibitors are summarized in Table 5 (AChE), Table 6 (α-glucosidase), and Table 7 (α-amylase). Among the phenolic constituents, rutin showed the most favorable binding energy towards all three enzymes (−10.46, −9.04, and −9.32 kcal/mol for AChE, α-glucosidase, and α-amylase, respectively). Rutin was also predicted to bind α-glucosidase and α-amylase more strongly than the reference inhibitor acarbose (−7.79 kcal/mol for both enzymes), whereas its affinity for AChE was lower than that of donepezil (−12.17 kcal/mol). The small phenolic compounds showed moderate binding energies, ranging from −6.31 to −7.54 kcal/mol for AChE, −5.60 to −5.89 kcal/mol for α-glucosidase, and −5.21 to −6.51 kcal/mol for α-amylase.

Binding to AChE

In AChE, the reference inhibitor donepezil spanned the active-site gorge from the catalytic anionic site (CAS) to the peripheral anionic site (PAS) through π–π stacking with Trp86, Trp286, Tyr341, and His447, π–cation interactions with Trp86 and Tyr337, an attractive charge interaction with Asp74, and a hydrogen bond with Phe295 **(Table 5; Figure 2a)**, in agreement with its crystallographic binding mode.[34] Rutin adopted a similar dual-site orientation **(Figure 2b)**. At the PAS, it formed conventional hydrogen bonds with Tyr72 and Asp74, a π–donor hydrogen bond and T-shaped π–π interaction with Tyr124, and π–π stacking with Trp286 and Tyr341, whereas at the CAS it formed hydrogen bonds with Trp86 and Glu202, carbon–hydrogen bonds with Ser203, T-shaped π–π stacking with Trp86, and a π–alkyl contact with His447. The small phenolic compounds were confined to the CAS **(Figure 2c–f)**. All four formed π–π stacking interactions with Trp86, the principal binding determinant of the quaternary ammonium group of acetylcholine. p-Coumaric and trans-cinnamic acids additionally formed hydrogen bonds with Tyr337 and Tyr341 and a π–anion interaction with Tyr337, whereas salicylic acid and vanillin formed hydrogen bonds with Glu202 (and, for salicylic acid, with the catalytic Ser203) and π–π stacking with the catalytic His447.

Table 5. Binding energies, ligand efficiencies, and interactions of the phenolic constituents of *G. dumosum* and the reference inhibitor with AChE (PDB: 4EY7)

Complex	ΔG (kcal/mol)	LE	Hydrogen bond interactions	Hydrophobic interactions	Electrostatic and other interactions
4EY7 @ Donepezil	−12.17	0.43	**Conv. H-bond** Phe295	**π–π stacked** Trp86(2), Trp286(2), Tyr341, His447 **π–sigma** Trp286, Phe338, Tyr341	**Attractive charge** Asp74 **π–cation** Trp86, Tyr337
4EY7 @	−10.46	0.24	**Conv. H-bond**	**π–π stacked**	–

Rutin			Tyr72, Asp74, Trp86, Tyr133, Glu202 **Carbon H-bond** Trp86, Tyr124, Ser203 **π–donor H-bond** Tyr124	Trp286, Tyr337, Tyr341(3) **π–π T-shaped** Trp86, Tyr124 **π–alkyl** His447	
4EY7 @ p-Coumaric acid	−7.54	0.63	**Conv. H-bond** Tyr133, Tyr337, Tyr341(2) **Carbon H-bond** Trp86	**π–π stacked** Trp86(2)	**π–anion** Tyr337
4EY7 @ trans-Cinnamic acid	−7.14	0.65	**Conv. H-bond** Tyr337, Tyr341 **Carbon H-bond** Trp86	**π–π stacked** Trp86(2)	**π–anion** Tyr337
4EY7 @ Salicylic acid	−6.54	0.65	**Conv. H-bond** Tyr133, Glu202, Ser203 **Carbon H-bond** Gly448	**π–π stacked** Trp86(2), His447	–
4EY7 @ Vanillin	−6.31	0.57	**Conv. H-bond** Glu202, Tyr337 **Carbon H-bond** Trp86, Tyr133, Gly448	**π–π stacked** Trp86(2), His447	–

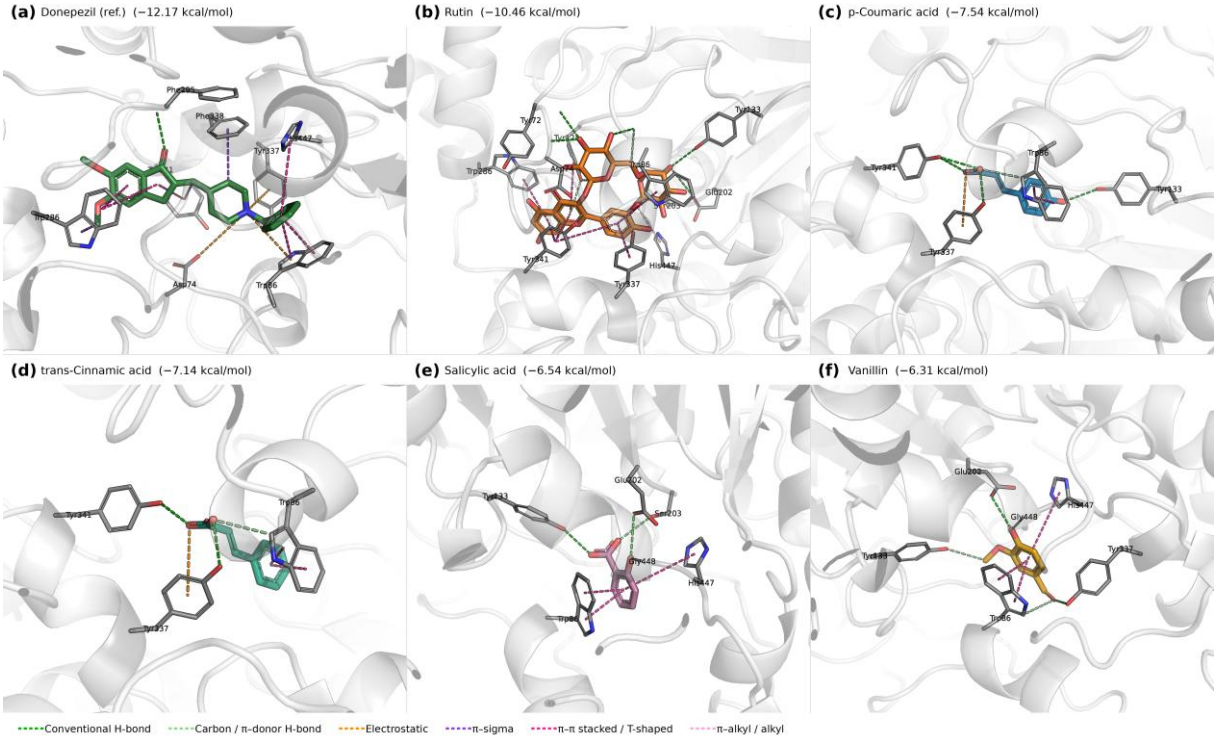

Figure **2**. Three-dimensional binding modes of (**a**) donepezil (reference), (**b**) rutin, (**c**) p-coumaric acid, (**d**) trans-cinnamic acid, (**e**) salicylic acid, and (**f**) vanillin in the active site of AChE (4EY7). Interaction types are indicated by the color code in the legend

Binding to α-glucosidase

In α-glucosidase, acarbose occupied the catalytic pocket and formed hydrogen bonds with Asp203, Thr205, Asn207, Arg526, Asp542, Thr544, and His600, a salt bridge with the acid/base catalyst Asp542, and attractive charge interactions between its protonated nitrogen and Asp203 and the catalytic nucleophile Asp443, together with π–alkyl contacts with Tyr299 and Phe575 **(Table 6; Figure 3a)**. Rutin bound in the same pocket **(Figure 3b)**, forming conventional hydrogen bonds with Asp203, Asp443, Trp406, His600, and Gln603, T-shaped π–π interactions with Trp406, π–π stacking with Phe450, and π–alkyl contacts with Trp441, Trp539, Phe575, and His600. All four small phenolics established a π–anion interaction with Asp443 **(Figure 3c–f)**. The carboxylate groups of salicylic, p-coumaric, and trans-cinnamic acids also formed attractive charge interactions with Arg526 and T-shaped π–π stacking with Tyr299, and salicylic acid and vanillin were further hydrogen-bonded to Asp542.

Table 6. Binding energies, ligand efficiencies, and interactions of the phenolic constituents of *G. dumosum* and the reference inhibitor with α-glucosidase (PDB: 2QMJ)

Complex	ΔG (kcal/mol)	LE	Hydrogen bond interactions	Hydrophobic interactions	Electrostatic and other interactions
2QMJ @ Acarbose	−7.79	0.18	**Conv. H-bond** Asp203, Thr205(2), Asn207, Arg526, Asp542, Thr544, His600 **Carbon H-bond** Asp443	**π–alkyl** Tyr299, Phe575	**Salt bridge** Asp542 **Attractive charge** Asp203, Asp443, Asp542
2QMJ @ Rutin	−9.04	0.21	**Conv. H-bond** Asp203(2), Trp406, Asp443, His600, Gln603(2)	**π–π stacked** Phe450 **π–π T-shaped** Trp406(2) **π–alkyl** Trp441, Trp539(2), Phe575, His600	–
2QMJ @ Salicylic acid	−5.89	0.59	**Conv. H-bond** Arg526, Asp542	**π–π T-shaped** Tyr299	**Attractive charge** Arg526 **π–anion** Asp443
2QMJ @ p-Coumaric acid	−5.89	0.49	**Conv. H-bond** His600	**π–π T-shaped** Tyr299	**Attractive charge** Arg526 **π–anion** Asp443
2QMJ @ trans-Cinnamic acid	−5.66	0.51	–	**π–π T-shaped** Tyr299	**Attractive charge** Arg526 **π–anion** Asp443
2QMJ@Vanillin	−5.60	0.51	**Conv. H-bond** Arg526, Asp542 Carbon H-bond Asp327	–	**π–anion** Asp443

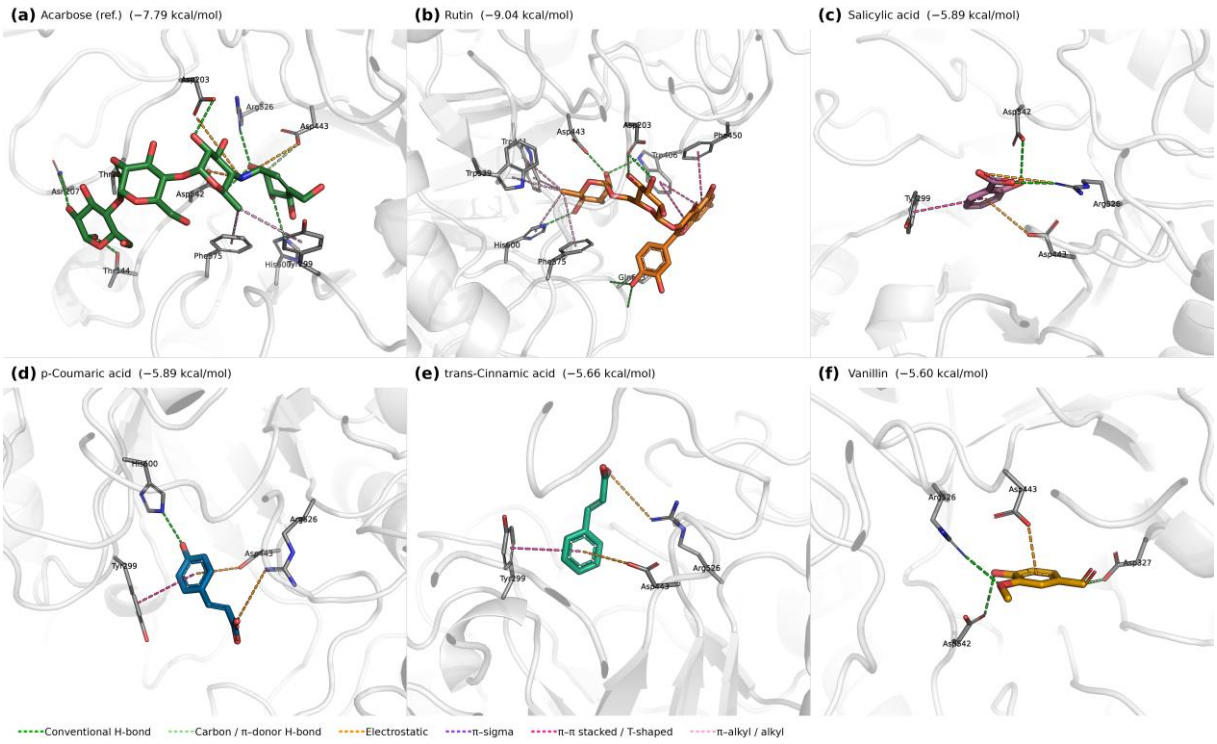

Figure **3**. Three-dimensional binding modes of (**a**) acarbose (reference), (**b**) rutin, (**c**) salicylic acid, (**d**) p-coumaric acid, (**e**) trans-cinnamic acid, and (**f**) vanillin in the active site of α-glucosidase (2QMJ). Interaction types are indicated by the color code in the legend.

Binding to α-amylase

In α-amylase, acarbose spanned the catalytic cleft and formed conventional hydrogen bonds with Trp59 and with the catalytic residue Asp300, carbon–hydrogen bonds with Thr163, Asp300, and the catalytic nucleophile Asp197, and a π–alkyl contact with Trp59 **(Table 7; Figure 4a)**. Rutin formed hydrogen bonds with both catalytic acidic residues, Glu233 and Asp300, as well as with Thr163, His299, and His305, and was further stabilized by π–π stacking with Tyr151, π–sigma interactions with Trp59 and Ile235, and π–alkyl contacts with Trp59, Leu162, Ile235, and His305 **(Figure 4b)**. All four small phenolics formed π–π interactions with Tyr62 **(Figure 4c–f)**. p-Coumaric acid was hydrogen-bonded to the catalytic nucleophile Asp197 and to Gln63 and Thr163, whereas vanillin and salicylic acid interacted with the catalytic Glu233 and with Asp197 or Asp300 through hydrogen bonds and π–anion interactions.

Table 7. Binding energies, ligand efficiencies, and interactions of the phenolic constituents of *G. dumosum* and the reference inhibitor with α-amylase (PDB: 2QV4)

Complex	ΔG (kcal/mol)	LE	Hydrogen bond interactions	Hydrophobic interactions	Electrostatic and other interactions
2QV4 @ Acarbose	−7.79	0.18	**Conv. H-bond** Trp59, Asp300(2) **Carbon H-bond**	**π–alkyl** Trp59(2)	-

			Thr163(2), Asp197(2), Asp300		
2QV4 @ Rutin	−9.32	0.22	**Conv. H-bond** Thr163, Glu233(2), His299, Asp300(2), His305	**π–π stacked** Tyr151 **π–sigma** Trp59, Ile235 **π–alkyl** Trp59, Leu162, Ile235, His305	–
2QV4 @ p-Coumaric acid	−6.51	0.54	**Conv. H-bond** Gln63, Thr163, Asp197	**π–π stacked** Tyr62	–
2QV4 @ trans-Cinnamic acid	−5.90	0.54	**Conv. H-bond** Gln63	**π–π stacked** Tyr62	**π–anion** Trp59(2)
2QV4 @ Vanillin	−5.38	0.49	**Conv. H-bond** Arg195, Glu233	**π–π stacked** Tyr62	**π–anion** Asp197
2QV4 @ Salicylic acid	−5.21	0.52	**Conv. H-bond** Glu233, Asp300	**π–π T-shaped** Tyr62	**π–anion** Asp300

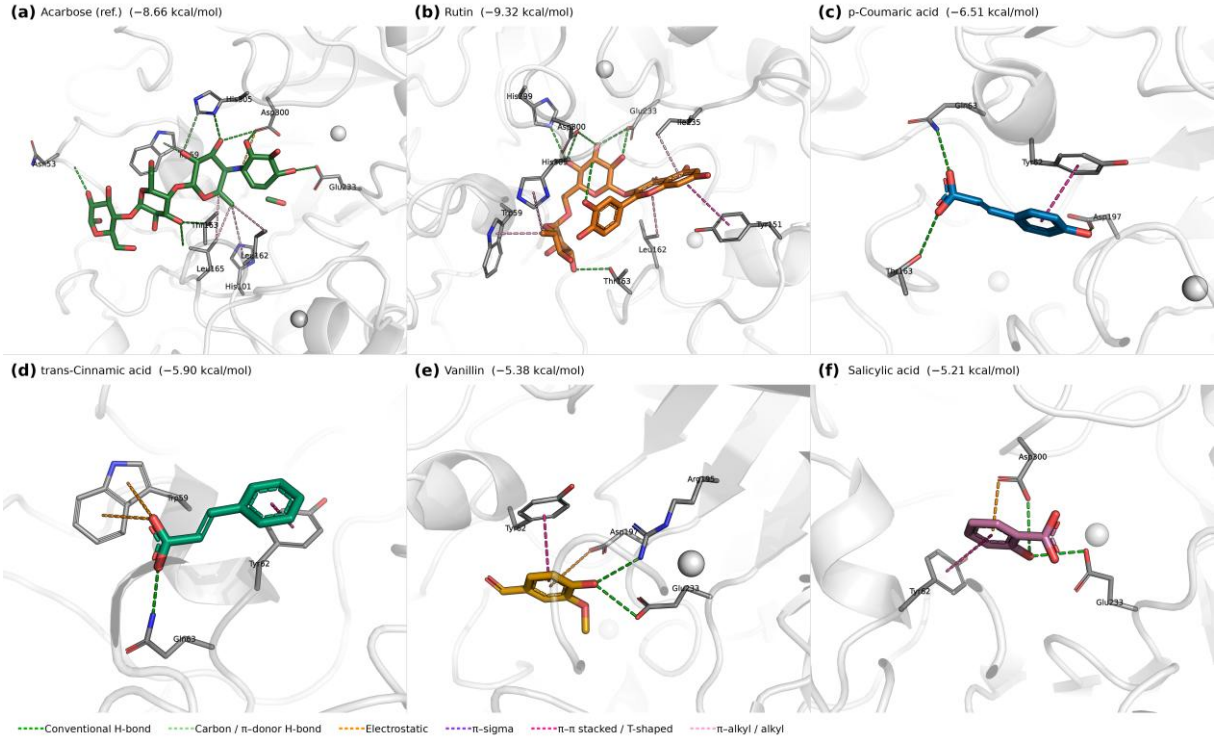

***Figure* 4**. Three-dimensional binding modes of (**a**) acarbose (reference), (**b**) rutin, (**c**) p-coumaric acid, (**d**) trans-cinnamic acid, (**e**) vanillin, and (**f**) salicylic acid in the active site of α-amylase (2QV4). Interaction types are indicated by the color code in the legend.

Comparison of rutin with the reference inhibitors

Because rutin showed the most favorable binding energies towards all three enzymes, its binding modes were compared in detail with those of the reference inhibitors **(Figure 5)**. In

AChE, six of the residues contacted by donepezil (Asp74, Trp86, Trp286, Tyr337, Tyr341, and His447) were also engaged by rutin, which additionally interacted with Tyr72, Tyr124, Tyr133, Glu202, and Ser203, consistent with a more extensive coverage of both the CAS and PAS. In α-glucosidase, rutin shared Asp203, Asp443, Phe575, and His600 with acarbose but extended towards a hydrophobic region lined by Trp406, Trp441, Phe450, and Trp539, which may explain its more favorable binding energy despite the absence of interactions with Arg526 and Asp542. In α-amylase, rutin and acarbose shared three residues, Trp59, Thr163, and the catalytic Asp300, indicating that both compounds occupy the same catalytic site, although rutin additionally engaged the second catalytic residue, Glu233.

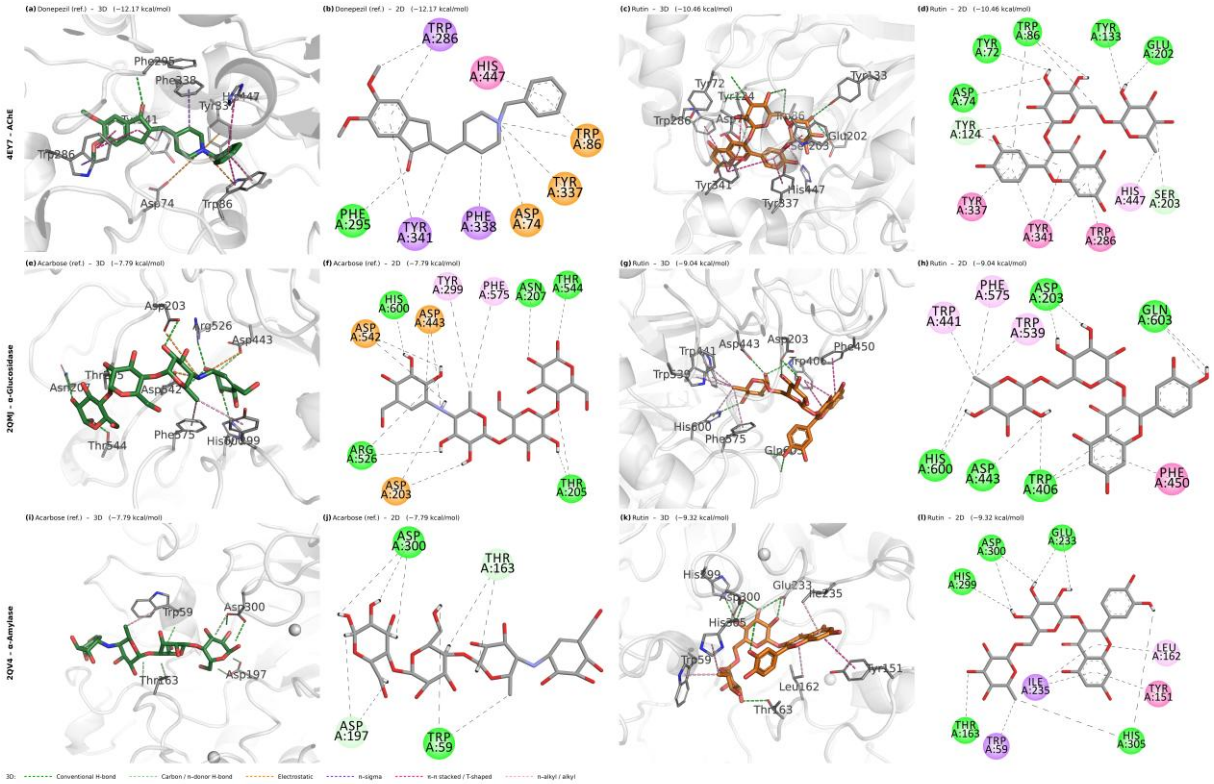

***Figure* 5.** Binding modes of the reference inhibitors and rutin: AChE with (a, b) donepezil and (c, d) rutin; α-glucosidase with (e, f) acarbose and (g, h) rutin; α-amylase with (i, j) acarbose and (k, l) rutin. For each pair, the 3D view is followed by the 2D diagram. Representation and *color code* of the 3D panels as in **Figure 2**; interaction types are listed in **Tables 5–7**

Because docking scores generally increase with molecular size, ligand efficiency (LE) was used to compare the compounds independently of the number of heavy atoms. LE values of approximately 0.3 kcal/mol per heavy atom or higher are generally considered favorable for lead-like compounds.[35] The small phenolics displayed high LE values (0.49–0.65), exceeding those of rutin (0.21–0.24) and the reference inhibitors (donepezil, 0.43; acarbose, 0.18–0.20). Although rutin achieved the strongest absolute binding through a large number of contacts, the

small phenolics bound more efficiently per atom, which is consistent with their compact structures and their high predicted absorption and, in the case of trans-cinnamic acid, CNS permeability **(Table 4)**.

These docking results are also consistent with the *in vitro* findings. The MeOH extract, which contained rutin together with p-coumaric, salicylic, and trans-cinnamic acids, showed stronger inhibition of all three enzymes than the DCM extract, which was dominated by vanillin **(Table 1; Table 2)**. In the docking analyses, rutin showed the strongest binding energies and vanillin among the weakest, suggesting that rutin and the phenolic acids may contribute more to the enzyme-inhibitory activity of the MeOH extract than vanillin. Docking scores, however, provide only an approximate estimate of binding affinity and do not account for protein flexibility or solvent effects. The stability of the selected complexes was therefore further examined by MD simulations and MM/GBSA calculations.

Molecular dynamics simulations

Docking evaluates a single static arrangement of each ligand in the active site and cannot show whether the complex persists in solution at physiological temperature. To test this, rutin and the reference inhibitor of each enzyme were simulated for 50 ns, and the last 25 ns of each trajectory were used for the quantitative comparisons below. The stability measures and binding free energies obtained for the six systems are collected in Tables 8 and 9.

All six systems reached equilibrium well within the first half of the simulation (Table 9). Backbone RMSD values settled between 0.14 and 0.22 nm and showed no drift thereafter, with α-amylase the most rigid of the three enzymes (**0.136 ± 0.010 nm** with acarbose, 0.145 ± 0.009 nm with rutin) and α-glucosidase the most mobile (0.224 ± 0.014 nm with acarbose). These are typical values for proteins of 496 to 863 residues and indicate that none of the enzymes was distorted by the bound ligand.

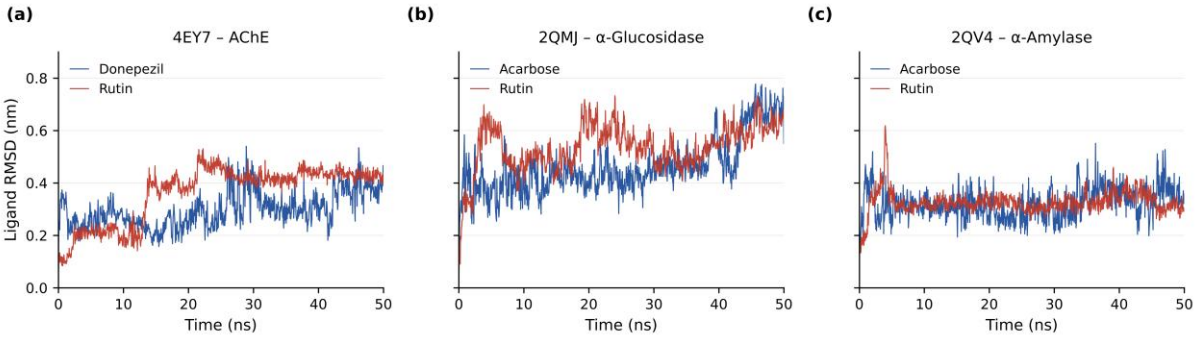

Figure **6**. Ligand RMSD during the 50 ns simulations, calculated after fitting each frame onto the protein: (a) 4EY7, (b) 2QMJ, (c) 2QV4.

Figure 6 shows how far each ligand moved relative to its binding site. Donepezil remained closest to its docked pose (0.340 ± 0.063 nm) and rutin stayed within 0.43 nm of it in the same gorge, after a stepwise shift at about 14 ns that was followed by a stable plateau. A rearrangement of this kind, once it is followed by a new plateau rather than a continued rise, reflects the ligand settling into a preferred orientation rather than leaving the site. In α-amylase the two ligands were indistinguishable (0.327 ± 0.034 nm for rutin against 0.336 ± 0.061 nm for acarbose) and traced the same narrow band through the second half of the run, while in α-glucosidase both fluctuated more (0.520 and 0.554 nm) and drifted upward over the final 10 ns.

The higher values obtained for both ligands in α-glucosidase should be read against their size and flexibility. Both molecules carry sugar units that remain exposed to solvent while the rest of the molecule occupies the catalytic site, so the RMSD of the whole molecule combines the displacement of the bound fragment with the free motion of the appended sugars. Donepezil, with 28 heavy atoms and a single compact scaffold, has no equivalent degree of freedom, which is part of why its RMSD is the lowest of the six. The same effect is visible in the crystal structure of 2QMJ, where the terminal glucose residues of acarbose have B-factors roughly twice those of the acarviosine moiety. The upward drift seen for both ligands over the last 10 ns in **Figure 6b** therefore does not necessarily mean that either compound is leaving the active site.

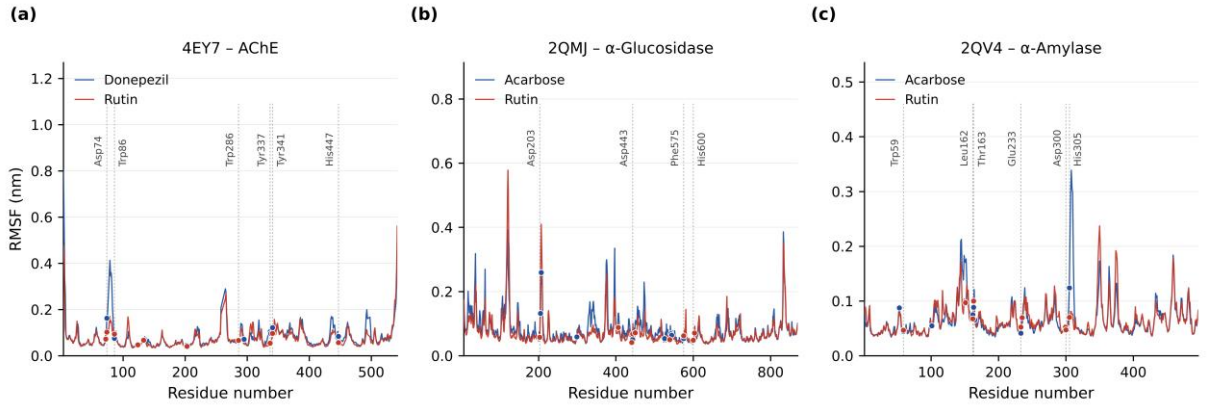

Figure **7**. Per-residue Cα RMSF over the final 25 ns: (a) 4EY7, (b) 2QMJ, (c) 2QV4. Dashed lines mark residues that contacted both ligands in the docking calculations; filled circles show the contact residues of each ligand.

Residue-level fluctuations are given in **Figure 7**. Mean Cα RMSF values were between 0.066 and 0.083 nm, and the largest peaks fall on the chain termini and on surface loops far from the active site, as expected. The residues identified as contacts in the docking analysis behave differently from the rest of the chain: almost all of them sit in the 0.04 to 0.10 nm range, below the mean of their own protein. In 4EY7 the aromatic residues that line the gorge, Trp86, Tyr337 and Tyr341, fluctuated by less than 0.09 nm with either ligand. The catalytic His447 was equally restrained. Rutin produced slightly lower fluctuations than the reference compound at most of these positions, which is consistent with its larger contact surface. The agreement between the docking contacts and the rigid regions of the simulated proteins supports the binding modes reported in **Tables 5 to 7**.

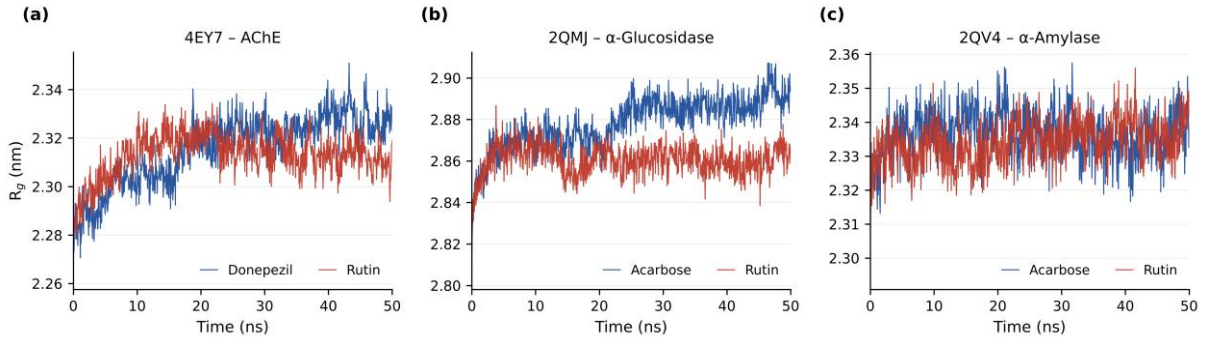

Figure **8**. Radius of gyration of the protein during the simulations: (a) 4EY7, (b) 2QMJ, (c) 2QV4.

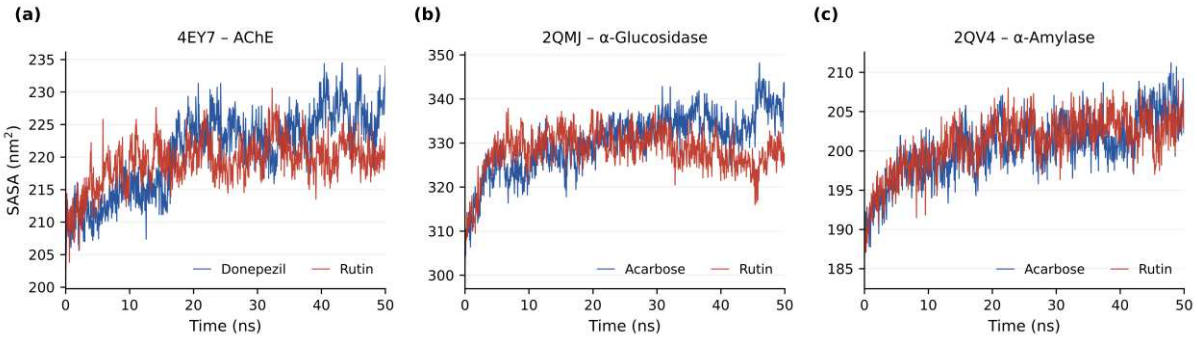

***Figure* 9**. Solvent-accessible surface area of the protein during the simulations: (a) 4EY7, (b) 2QMJ, (c) 2QV4.

Global compactness and surface exposure, shown in **Figures 8** and **9**, changed very little. Radii of gyration varied by less than 0.01 nm within each system over the final 25 ns, and solvent-accessible surface areas were constant to within about 2% (224.8 ± 3.5 nm² for 4EY7 with donepezil, 334.9 ± 3.8 nm² for 2QMJ with acarbose, 202.9 ± 2.1 nm² for 2QV4 with rutin). The small offsets between the two ligands of a given enzyme, such as the 0.027 nm difference in Rg between the acarbose and rutin complexes of α-glucosidase, are at the level of normal thermal breathing and should not be over-interpreted. Neither ligand opened or collapsed the fold it was bound to.

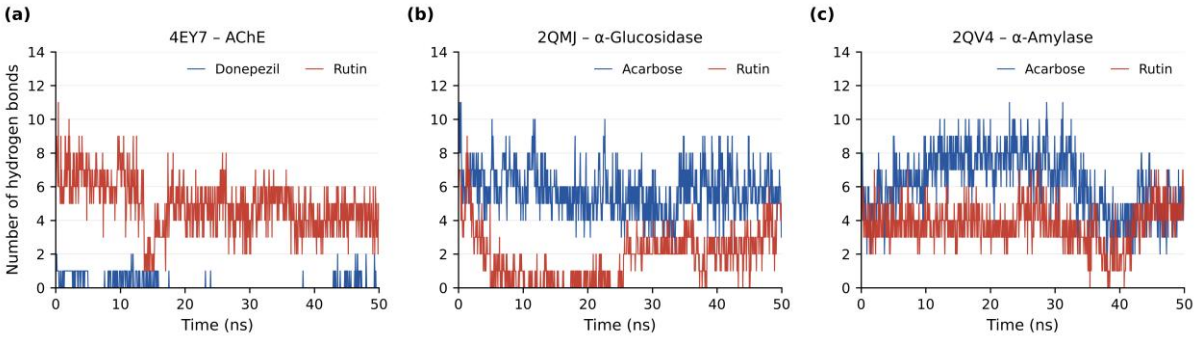

***Figure* 10**. Number of hydrogen bonds between protein and ligand during the simulations: (a) 4EY7, (b) 2QMJ, (c) 2QV4.

Hydrogen bonding separates the ligands much more sharply (**Figure 10**). Acarbose maintained 5.50 ± 1.36 bonds with α-glucosidase and 5.62 ± 1.88 with α-amylase, which is what its many hydroxyl groups allow. Rutin formed fewer in those two enzymes (2.46 and 3.62), but in AChE it reached 4.49 ± 1.18 while donepezil formed essentially none (0.08 ± 0.31, with no hydrogen bond present in 81% of the frames). Donepezil therefore does not depend on hydrogen bonding for its affinity. Its affinity comes from aromatic stacking against Trp86 and Trp286 and from the cation-π interaction between its protonated piperidine nitrogen and the aromatic wall of the gorge, so the near-zero count in **Figure 10a** describes its binding mode rather than a weakness

of the complex. The energy decomposition below separates the two compounds along the same lines.

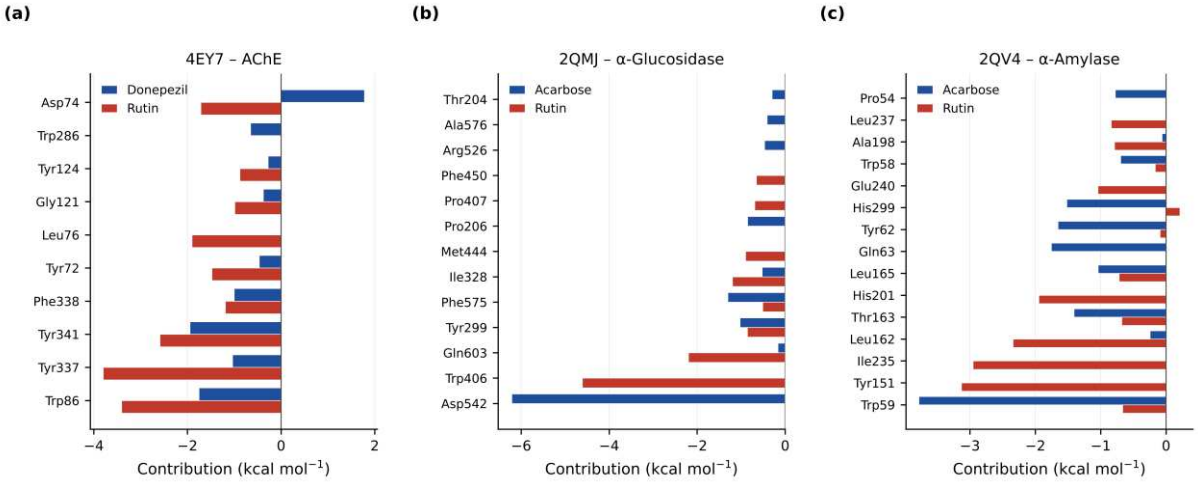

***Figure* 11**. Per-residue decomposition of the MM/GBSA binding free energy. The residues contributing most to binding are shown for (a) 4EY7, (b) 2QMJ, (c) 2QV4.

Binding free energies and their components are collected in **Table 8**. Two limitations apply to these values. The conformational entropy term was not calculated, and the generalized Born treatment handles charged ligands less reliably than neutral ones, so the values are useful for comparison but are not estimates of absolute affinity.[19,36] The size dependence matters here as well: because the entropic penalty of freezing a flexible molecule is omitted, MM/GBSA systematically favors larger ligands. Rutin and acarbose have 43 and 44 heavy atoms respectively, while donepezil has 28, so rutin and acarbose can be compared with each other on reasonably equal terms, whereas the rutin–donepezil comparison cannot be read as a ranking of affinity.

Within these limits, the two carbohydrate-hydrolyzing enzymes behaved differently. In α-glucosidase acarbose bound more strongly than rutin (−26.24 ± 6.55 against −16.20 ± 6.05 kcal/mol), in agreement with the docking scores and with its established inhibitory activity. In α-amylase the order was reversed, rutin reaching −29.80 ± 6.10 kcal/mol against −24.36 ± 11.17 for acarbose. The acarbose value still carries the widest spread in the table, which comes from the swings of its electrostatic and polar solvation terms (−130.43 ± 48.34 and 141.16 ± 50.89 kcal/mol); the difference between the two ligands in that enzyme therefore lies within the uncertainty of the method and should not be read as a ranking.

The composition of the binding energies differs more than their totals. For rutin, the van der Waals term dominates in all three enzymes (−31.97 to −50.09 kcal/mol) while the electrostatic

and polar solvation contributions nearly cancel. For acarbose and donepezil, both of which carry a positive charge, the electrostatic term is an order of magnitude larger (−258.15 kcal/mol for donepezil, −535.66 kcal/mol for acarbose in α-glucosidase) but is almost entirely offset by the desolvation penalty. This cancellation of two large opposing terms is the main source of uncertainty in the acarbose complexes, whose standard deviations are the largest in **Table 8**.

Figure 11 identifies which residues drive the interaction. In AChE the main contributors to donepezil binding were Tyr341 (−1.95 kcal/mol), Trp86 (−1.75) and Tyr337 (−1.04), the same aromatic residues seen in the docking analysis and in **Figure 7a** as the least mobile part of the gorge. Rutin engaged the same residues more strongly (Tyr337 −3.80, Trp86 −3.41, Tyr341 −2.59 kcal/mol) and additionally recruited Leu76 and Tyr72. Asp74 behaved differently for the two compounds, contributing favorably to rutin binding (−1.71 kcal/mol) but opposing donepezil (+1.78 kcal/mol), a sign that the charged carboxylate pays a desolvation cost it does not recover when the cationic ligand is bound. In α-glucosidase, Asp542 accounted for a quarter of the total acarbose energy (−6.21 kcal/mol), whereas rutin relied mainly on Trp406 (−4.61) and Gln603 (−2.20). In α-amylase, acarbose was held mainly by Trp59 (−3.78 kcal/mol), with Gln63, Tyr62, His299 and Thr163 contributing between −1.76 and −1.41 kcal/mol, while rutin bound to a partly different set centered on Tyr151, Ile235 and Leu162 (−3.13, −2.95 and −2.34 kcal/mol). The catalytic carboxylates behaved alike for both compounds, making small positive contributions in each case (Asp197 +0.69 and Asp300 +0.62 for acarbose; +0.73 and +1.67 for rutin). Both ligands hydrogen-bond to these residues in the docked poses and stay within 4 Å of them throughout the simulation, but the strongly favorable electrostatic term that the charged side chains generate is almost entirely repaid as a desolvation penalty in the generalized Born model, leaving a small net cost. Their contribution to binding is therefore better judged from the contact analysis in Table 7 than from the decomposition.

The simulations therefore show that rutin forms complexes of comparable stability to the reference inhibitors in all three enzymes, with no dissociation over 50 ns, but that its binding relies on a different balance of forces: extensive van der Waals contact and hydrogen bonding with aromatic and polar residues rather than the close electrostatic engagement of a catalytic carboxylate that acarbose achieves in α-glucosidase. This is consistent with the inhibitory activity measured for the extracts and with the predicted pharmacokinetic profile of rutin, which points to a local action in the gastrointestinal tract rather than systemic exposure.[29] Integrated docking–MD–MM/GBSA pipelines applied to other endemic Anatolian species have likewise converged on a single dominant phenolic as the principal predicted contributor to multi-target

enzyme inhibition — chlorogenic acid in both *G. komagenensis* and *A. fumariifolia* — which lends methodological support to the identification of rutin in that role here.[20,25]

Table 8. MM/GBSA binding free energies and their components for the six simulated complexes, averaged over 101 snapshots from the final 25 ns of each trajectory (kcal/mol, mean ± SD)

Complex	ΔE_{vdW}	ΔE_{elec}	ΔG_{polar}	$\Delta G_{nonpolar}$	ΔG_{bind}
4EY7 – Donepezil	−38.17 ± 2.99	−258.15 ± 14.90	281.29 ± 16.00	−5.07 ± 0.44	−20.10 ± 2.19
4EY7 – Rutin	−50.09 ± 3.50	−34.22 ± 6.66	58.84 ± 4.73	−7.14 ± 0.31	−32.61 ± 4.35
2QMJ – Acarbose	−21.55 ± 5.14	−535.66 ± 18.73	535.56 ± 16.91	−4.58 ± 0.62	−26.24 ± 6.55
2QMJ – Rutin	−31.97 ± 3.76	−35.82 ± 14.68	56.44 ± 11.95	−4.84 ± 0.57	−16.20 ± 6.05
2QV4 – Acarbose	−29.78 ± 11.66	−130.43 ± 48.34	141.16 ± 50.89	−5.31 ± 2.03	−24.36 ± 11.17
2QV4 – Rutin	−41.70 ± 3.49	−45.39 ± 10.91	63.81 ± 6.67	−6.52 ± 0.57	−29.80 ± 6.10

Table 9. Stability measures averaged over the final 25 ns of each simulation (mean ± SD)

Complex	Backbone RMSD (nm)	Ligand RMSD (nm)	Cα RMSF (nm)	R_g (nm)	SASA (nm²)	H-bonds
4EY7 – Donepezil	0.197 ± 0.011	0.340 ± 0.063	0.083 ± 0.064	2.325 ± 0.007	224.8 ± 3.5	0.08 ± 0.31
4EY7 – Rutin	0.177 ± 0.010	0.428 ± 0.021	0.074 ± 0.049	2.313 ± 0.006	220.5 ± 2.6	4.49 ± 1.18
2QMJ – Acarbose	0.224 ± 0.014	0.520 ± 0.108	0.083 ± 0.047	2.888 ± 0.006	334.9 ± 3.8	5.50 ± 1.36
2QMJ – Rutin	0.200 ± 0.014	0.554 ± 0.063	0.075 ± 0.051	2.861 ± 0.006	328.2 ± 3.6	2.46 ± 1.07
2QV4 – Acarbose	0.136 ± 0.010	0.336 ± 0.061	0.067 ± 0.037	2.336 ± 0.007	202.8 ± 2.8	5.62 ± 1.88
2QV4 – Rutin	0.145 ± 0.009	0.327 ± 0.034	0.066 ± 0.028	2.336 ± 0.006	202.9 ± 2.1	3.62 ± 1.43

Conclusion

This study provides an integrated evaluation of the phytochemical composition and biological activities of *Galium dumosum* extracts. LC–MS/MS analysis revealed distinct solvent-dependent profiles, with the MeOH extract containing a greater diversity of phenolic compounds, whereas the DCM extract was predominantly characterized by vanillin. Both extracts inhibited acetylcholinesterase, α-glucosidase, and α-amylase, and both scavenged

$ABTS^{\bullet+}$ and reduced Fe^{3+}; the MeOH extract was the more active of the two in every assay, although the reference antioxidants remained more potent in the ABTS assay.

Molecular docking identified rutin as the constituent with the most favorable predicted binding to the three enzymes, and MD simulations showed that its complexes remained stable over 50 ns. These computational findings provide complementary evidence for the possible contribution of phenolic constituents to the observed enzyme inhibitory activities, although experimental validation is still required.

Regarding cytotoxicity, the MeOH extract did not produce significant reductions in the viability of MIA PaCa-2 pancreatic cancer cells or HUVECs under the tested conditions. The findings therefore do not support a direct anticancer effect of the extract in the investigated cell models. *G. dumosum* appears to be a promising source of phenolic compounds with antioxidant and enzyme inhibitory potential. Further studies focusing on the isolation of active constituents, enzyme inhibition mechanisms, and in vivo evaluation are needed to clarify its biological significance and potential applications.

Methods

Plant material

The aerial parts of *Galium dumosum* Boiss. were collected in June 2024 from a restricted area near the Gürlevik water resources in Adıyaman, Türkiye, at an altitude of 1200–1250 m, in rocky habitats. The plant material was identified by the plant taxonomist Dr. Ö. Kılıç using the descriptions in *Flora of Turkey and the East Aegean Islands*, Volume 7.[7] The collected material was dried under herbarium conditions and subsequently used for extraction and phytochemical analyses. A voucher specimen was deposited in the Department of Pharmaceutical Botany, Faculty of Pharmacy, Adıyaman University, Türkiye, under voucher number 2987. Collection of the plant material complied with relevant institutional, national, and international guidelines and legislation.

Preparation of plant extracts

The aerial parts of *Galium dumosum* were dried, powdered, and extracted separately with methanol (MeOH) and dichloromethane (DCM). Briefly, 20 g of powdered plant material was macerated in 200 mL of each solvent (1:10, w/v) at room temperature for 24 h with continuous stirring. The extracts were filtered through Whatman filter paper and concentrated under reduced pressure using a rotary evaporator. The resulting dried extracts were weighed,

transferred to glass vials, and stored at −20 °C until further analysis. Stock solutions were prepared by dissolving 1 mg of each extract in 10 mL of the corresponding solvent.[33]

LC–MS/MS analysis of phenolic compounds

The qualitative and quantitative characterization of phenolic compounds in the methanol and dichloromethane extracts of *G. dumosum* was performed using an Agilent 1260 Infinity II liquid chromatography system coupled to an Agilent 6460 Triple Quadrupole mass spectrometer (Agilent Technologies, Santa Clara, CA, USA) equipped with an electrospray ionization (ESI) source. Chromatographic separation was achieved using a Poroshell 120 EC-C18 column (50 × 4.6 mm i.d., 2.7 µm particle size) maintained at 30 °C. The mobile phase consisted of solvent A (water containing 0.1% formic acid and 5 mM ammonium formate) and solvent B (acetonitrile containing 0.1% formic acid). The flow rate was 0.4 mL/min, and the injection volume was 4 µL.

The gradient elution program was as follows: 85% A and 15% B at 0 min; 75% A and 25% B at 5 min; 25% A and 75% B at 15 min; and 0% A and 100% B at 16 min. The composition was maintained at 100% B until 20 min, followed by a return to the initial conditions (85% A/15% B) at 22 min. The initial mobile-phase composition was maintained until 40 min for column re-equilibration. The total run time was 40 min.

For sample preparation, 50 mg of each dried extract was accurately weighed into a 2-mL Eppendorf tube and dissolved in 1 mL of acetonitrile–methanol–water (1:1:1, v/v/v). The samples were vortex-mixed until dissolution. When complete dissolution was not achieved, the samples were further treated in an ultrasonic bath. Subsequently, 0.8 mL of n-hexane was added, and the samples were mixed and centrifuged at 7000 rpm for 5 min. The lower polar phase was collected, diluted four-fold, and filtered through a 0.25-µm membrane filter prior to LC–MS/MS analysis.

Mass spectrometric detection was performed in multiple-reaction-monitoring (MRM) mode using both positive and negative ESI modes. The source parameters were set as follows: gas temperature, 300 °C; drying gas flow, 11 L/min; nebulizer pressure, 15 psi; and capillary voltage, 4000 V. Compound-specific precursor-to-product ion transitions, dwell times, fragmentor voltages, collision energies, and ionization polarities are presented in Table 1. Phenolic compounds were identified based on their retention times and characteristic MRM transitions obtained from authentic analytical standards. Quantification was performed using the corresponding external standards under identical chromatographic and mass spectrometric

conditions, and the results were expressed as μg/g of extract. The analytical procedure was performed according to previously reported LC–MS/MS methodologies with appropriate modifications.[25,37]

Cell culture conditions

Human pancreatic cancer cells (MIA PaCa-2; ATCC CRL-1420) and human umbilical vein endothelial cells (HUVECs; ATCC CRL-1730) were obtained from the American Type Culture Collection (ATCC). MIA PaCa-2 cells were cultured in high-glucose Dulbecco's Modified Eagle Medium (DMEM) supplemented with 10% (v/v) fetal bovine serum (FBS), 2.5% (v/v) horse serum, and 1% (v/v) penicillin–streptomycin. HUVECs were maintained in high-glucose DMEM supplemented with 10% (v/v) FBS and 1% (v/v) penicillin–streptomycin. Both cell lines were incubated at 37 °C in a humidified atmosphere containing 5% CO_2 and subcultured at 70–80% confluence using 0.25% trypsin–EDTA.

Cell viability assay

Cell viability was assessed using the MTT assay. Cells were seeded in 96-well plates at a density of 1.5×10^4 cells/well and treated with various concentrations of the methanol (MeOH) extract (62.5–1000 μg/mL) for 24 and 48 h. Following treatment, MTT solution was added, and the plates were incubated to allow formazan crystal formation. The resulting crystals were dissolved in DMSO, and absorbance was measured at 570 nm using an RT-2100C microplate reader (Rayto Life and Analytical Sciences Co., Ltd., Shenzhen, China). A vehicle control containing the corresponding concentration of DMSO without extract was included. Cell viability was expressed as a percentage of the untreated control.

Seeding density optimization

To determine the optimal seeding density, cells were plated across a range of 3,000 to 15,000 cells/well, and absorbance was measured at 24 and 48 h. A density of 15,000 cells/well was selected for all subsequent experiments.

Statistical analysis

All experiments were performed in triplicate, and data are expressed as the mean ± standard deviation (SD). Statistical significance was evaluated using one-way or two-way ANOVA followed by Tukey's multiple-comparison test, with $p < 0.05$ considered statistically significant. IC_{50} values were estimated by four-parameter logistic nonlinear regression in GraphPad Prism (GraphPad Software, San Diego, CA, USA).

Antioxidant assays

ABTS radical cation scavenging assay

The antioxidant activity of the extracts was evaluated using the ABTS radical cation ($ABTS^{\bullet+}$) scavenging assay following the method of Re et al.[38] with modifications described previously.[21] Briefly, the $ABTS^{\bullet+}$ radical was generated by mixing 7 mM ABTS solution with 2.45 mM potassium persulfate ($K_2S_2O_8$) solution, followed by incubation in the dark at room temperature for 12–16 h. Prior to the assay, the resulting $ABTS^{\bullet+}$ solution was diluted with ethanol to obtain an absorbance of 0.70 ± 0.02 at 734 nm.

For the assay, 20–100 µL of the extracts at different concentrations was added to 2 mL of the diluted $ABTS^{\bullet+}$ solution and incubated at room temperature in the dark for 6–10 min. The decrease in absorbance was subsequently measured at 734 nm using a spectrophotometer. Ascorbic acid (AA), butylated hydroxyanisole (BHA), and butylated hydroxytoluene (BHT) were used as reference antioxidants under identical experimental conditions. The $ABTS^{\bullet+}$ radical scavenging activity was expressed as percentage inhibition relative to the control according to the following equation[39]:

$$\text{ABTS}^{\cdot+} \text{ scavenging activity (\%)} = \frac{A_0 - A_1}{A_0} \times 100$$

where A_0 represents the absorbance of the control reaction and A_1 represents the absorbance in the presence of the extract or reference antioxidant. All measurements were performed in triplicate.

FRAP assay

The ferric reducing antioxidant power (FRAP) assay was performed to evaluate the reducing capacity of the extracts according to Oyaizu (1986),[40] with minor modifications.[41] The FRAP reagent was freshly prepared by mixing 300 mM acetate buffer (pH 3.6), 10 mM 2,4,6-tripyridyl-s-triazine (TPTZ) solution prepared in 40 mM HCl, and 20 mM $FeCl_3 \cdot 6H_2O$ solution at a ratio of 10:1:1 (v/v/v) and warmed to 37 °C before use.

For the assay, 100 µL of each extract at different concentrations was mixed with 3 mL of the FRAP reagent and incubated at 37 °C for 4–10 min. The increase in absorbance was measured at 700 nm against an appropriate reagent blank using a spectrophotometer. The reducing capacity of the extracts was determined from the concentration–absorbance curves. Ascorbic

acid (AA), BHA, and BHT were used as reference antioxidants under identical experimental conditions. All measurements were performed in triplicate.

Enzyme inhibition assays

Acetylcholinesterase (AChE) inhibition assay

AChE inhibitory activity of the *G. dumosum* extracts was assessed using a modified Ellman spectrophotometric procedure. Briefly, the enzyme was pre-incubated with different concentrations of the extract for a predetermined period at room temperature. The reaction was subsequently initiated by adding acetylthiocholine iodide, while DTNB [5,5′-dithiobis-(2-nitrobenzoic acid)] was used as the chromogenic reagent. The enzymatic hydrolysis was monitored by measuring the absorbance at 412 nm. The inhibitory activity was expressed as a percentage relative to the enzyme control, and IC_{50} values were calculated from concentration–response curves using nonlinear regression analysis.[42,43]

α-Amylase inhibition assay

The inhibitory effect of the *G. dumosum* extracts on α-amylase was determined using a starch hydrolysis assay with minor modifications. The extracts were prepared at 10 mg/mL in ethanol–water (1:1, v/v). The reaction mixture containing soluble starch, phosphate buffer (pH 6.9), and the extract was pre-incubated before the addition of α-amylase. Following enzymatic incubation, the reaction was terminated with hydrochloric acid, and the absorbance was measured at 580 nm. Acarbose was used as the reference inhibitor.[44]

α-Glucosidase inhibition assay

α-Glucosidase inhibitory activity was determined using a colorimetric method based on the hydrolysis of p-nitrophenyl-α-D-glucopyranoside (pNPG). The enzyme was incubated with different concentrations of the extract, followed by the addition of pNPG and further incubation at 37 °C. The formation of p-nitrophenol was monitored at 405 nm. Acarbose was used as the positive control.[45]

For all enzyme assays, inhibition was calculated using the following equation:

$$\textbf{Inhibition (\%)} = [(A_0 - A_1) / A_0] \times 100$$

where A_0 and A_1 represent the absorbance values obtained in the absence and presence of the extract, respectively. IC_{50} values were calculated from concentration–response curves using nonlinear regression analysis.

In silico analyses

Ligand selection and preparation

Five phenolic constituents quantified in the *G. dumosum* extracts by LC–MS/MS, namely rutin, p-coumaric acid, vanillin, salicylic acid, and trans-cinnamic acid, were selected for in silico analysis. Donepezil and acarbose, the reference inhibitors used in the *in vitro* assays, were included as positive controls in the molecular docking and MD analyses. The structures of the five phenolic compounds and acarbose were retrieved from the PubChem database as isomeric SMILES (CIDs: rutin, 5280805; p-coumaric acid, 637542; vanillin, 1183; salicylic acid, 338; trans-cinnamic acid, 444539; acarbose, 41774). Three-dimensional coordinates were generated, ionization states at physiological pH (7.4) were assigned, and the structures were energy-minimized with the MMFF94 force field using Open Babel 3.2.1.[46] Under these conditions, the carboxylic acid groups of p-coumaric, salicylic, and trans-cinnamic acids were deprotonated, and the secondary amine nitrogen of acarbose was protonated. The co-crystallized ligands of the three enzyme structures (donepezil in 4EY7, acarbose in 2QMJ, and the acarbose-derived oligosaccharide in 2QV4) were extracted directly from the crystal coordinates. Their bond orders were verified against the PDB chemical component definitions and corrected where necessary using RDKit,[47] and the ligands were protonated in the same way, with the piperidine nitrogen of donepezil and the amine nitrogens of the acarbose-type ligands carrying a positive charge. Donepezil and acarbose in their crystallographic forms served both as validation ligands and as reference compounds for AChE and α-glucosidase, respectively, whereas acarbose prepared from PubChem was used as the reference compound for α-amylase. All ligands were converted to PDBQT format with Open Babel, which assigns Gasteiger charges, merges non-polar hydrogens, and defines rotatable bonds.

Drug-likeness and ADMET prediction

The drug-likeness of the ligands was evaluated according to Lipinski's rule of five,[16] which considers molecular weight (≤ 500 Da), lipophilicity (Log P ≤ 5), number of hydrogen-bond donors (≤ 5), and number of hydrogen-bond acceptors (≤ 10); compounds with no more than one violation were regarded as drug-like. The molecular descriptors required for this evaluation, together with the ADMET profiles of the compounds, were obtained from the pkCSM web server using the canonical SMILES of each ligand.[28] The predicted ADMET parameters were:

- Absorption: water solubility, Caco-2 permeability, human intestinal absorption, skin permeability, and P-glycoprotein substrate/inhibitor status.

- Distribution: steady-state volume of distribution (VDss), fraction unbound, blood–brain barrier (BBB) permeability, and central nervous system (CNS) permeability.
- Metabolism: substrate and inhibitor status for cytochrome P450 isoforms CYP1A2, CYP2C9, CYP2C19, CYP2D6, and CYP3A4.
- Excretion: total clearance and renal OCT2 substrate status.
- Toxicity: AMES mutagenicity, maximum tolerated dose, hERG inhibition, oral rat acute toxicity (LD_{50}), hepatotoxicity, and skin sensitization.

Protein preparation

The crystal structures of human AChE in complex with donepezil (PDB ID: 4EY7, 2.35 Å), the N-terminal catalytic subunit of human maltase-glucoamylase in complex with acarbose (PDB ID: 2QMJ, 1.90 Å), and human pancreatic α-amylase in complex with acarbose (PDB ID: 2QV4, 1.97 Å) were retrieved from the RCSB Protein Data Bank.[48] Chain A of each structure was used. Water molecules, co-crystallized ligands, glycosylation residues, and crystallization additives were removed, and for residues with alternate conformations only the first conformer was retained. No missing side-chain atoms were present in the structures. For α-amylase, the structural Ca^{2+} ion was retained, and the nitrite ion occupying the anion-binding site in 2QV4 was replaced by a Cl^- ion at the same position to reproduce the physiological chloride-activated state of the enzyme. In addition, the N-terminal pyroglutamate residue of 2QV4, located approximately 18 Å from the active site, was converted to glutamine. Polar hydrogen atoms were added at pH 7.4, Gasteiger charges were assigned, and the receptors were converted to rigid PDBQT format using Open Babel.[46,48]

Molecular docking

Molecular docking was performed with AutoDock Vina 1.2.5.[49,50] For each enzyme, the grid box was centered on the centroid of the co-crystallized ligand and sized to fully enclose the active site. Box dimensions were **24 × 20 × 21** Å for AChE, which covers both the catalytic anionic site and the peripheral anionic site, **20 × 20 × 27** Å for α-glucosidase, and **26 × 23 × 22** Å for α-amylase. Docking was carried out with an exhaustiveness of 32 and a fixed random seed (42), generating nine binding poses per ligand with a maximum energy difference of 3 kcal/mol, and the pose with the lowest binding energy was selected for further analysis. To validate the docking protocol, the co-crystallized ligand of each structure was re-docked into its binding site, and the symmetry-corrected heavy-atom root-mean-square deviation (RMSD)

between the docked and crystallographic poses was calculated without structural superposition; an RMSD ≤ 2.0 Å was considered acceptable. Because docking scores tend to increase with molecular size, ligand efficiency (LE = −ΔG/N, where N is the number of heavy atoms) was also calculated to allow a size-independent comparison of the compounds. Protein–ligand interactions, including conventional and carbon–hydrogen bonds, π–π, π–sigma, π–alkyl, and electrostatic interactions, were identified with BIOVIA Discovery Studio Visualizer 2019,[51] which was also used to generate the two-dimensional interaction diagrams. Three-dimensional views of the complexes were rendered with PyMOL 2.5.[52]

Molecular dynamics simulations

The best-scoring docking poses of rutin and of the reference inhibitors (donepezil for AChE; acarbose for α-glucosidase and α-amylase) were subjected to 50 ns all-atom MD simulations in explicit solvent, giving six protein–ligand systems in total. Simulations were performed with GROMACS 2025.3[53] with GPU acceleration.

Systems were assembled with CHARMM-GUI Solution Builder[54] using the CHARMM36m force field for the protein[55] and CGenFF for the ligands.[56] Disulfide bridges were defined according to the corresponding crystal structures, and the crystallographic Ca^{2+} and Cl^{-} ions of α-amylase, which are required for its structural integrity and activity, were retained. Each complex was placed in a rectangular box with a 10 Å solute–edge distance, solvated with TIP3P water[57] and neutralized with 0.15 M NaCl. After steepest-descent energy minimization, the systems were equilibrated for 100 ps in the NVT ensemble at 310 K using the velocity-rescaling thermostat[58] and for a further 100 ps in the NPT ensemble at 1 bar with the stochastic cell-rescaling barostat,[59] with position restraints on the solute that were released for the production run. Production simulations of 50 ns were carried out at 310 K and 1 bar using the Parrinello–Rahman barostat.[60] Bonds to hydrogen atoms were constrained with LINCS,[61] allowing a 2 fs time step; electrostatics were treated with the particle-mesh Ewald method[62] with a 1.2 nm cut-off, and van der Waals interactions were force-switched between 1.0 and 1.2 nm. Coordinates were saved every 50 ps.

After correction for periodic boundary effects, ligand RMSD was calculated following least-squares fitting onto the protein, so that the values reflect displacement relative to the binding site rather than internal flexibility. Per-residue Cα RMSF, radius of gyration, solvent-accessible surface area and the number of protein–ligand hydrogen bonds (0.35 nm and 30° cut-offs) were

also determined, with averages taken over the final 25 ns, by which time all systems had equilibrated.

MM/GBSA binding free energy calculations

Binding free energies (ΔG_{bind}) were calculated with the MM/GBSA method implemented in gmx_MMPBSA[63,64] on 101 snapshots taken at regular intervals from the last 25 ns of each production trajectory, using the modified generalized Born model of Onufriev et al. (igb = 5),[65] a salt concentration of 0.15 M, and a temperature of 310 K. ΔG_{bind} was decomposed into van der Waals, electrostatic, polar solvation, and nonpolar solvation contributions, and per-residue decomposition was carried out for all residues within 5 Å of the ligand to identify those contributing most to binding. The conformational entropy term was not included, so the values are interpreted as relative rather than absolute binding free energies.[19]

Data availability

The datasets generated and analysed during this study are available from the corresponding author on reasonable request.

References

1. Kilic, O. & Bagci, E. An ethnobotanical survey of some medicinal plants in Keban (Elazığ-Turkey). *J. Med. Plants Res.* **7**, 1675–1684 (2013).
2. Friščić, M., Štibrić Baglama, M., Milović, M., Hazler Pilepić, K. & Maleš, Ž. Content of bioactive constituents and antioxidant potential of *Galium* L. species. *Croat. Chem. Acta* **91** (2018). https://doi.org/10.5562/cca3379
3. Yıldırımlı, Ş. The chorology of the Turkish species of Rubiaceae and Rutaceae families. *Ot Sist. Bot. Derg.* **18**, 173–204 (2011).
4. Ergun, F., Deliorman, D., Velioglu, A., Sener, B. & Bozok Johansson, C. Antimicrobial activities of *Galium* species. *J. Fac. Pharm. Gazi Univ.* **16**, 7–11 (1999).
5. Tekeli, Y., Kılıç, Ö. & Altuner, E. E. DNA protective assay and some biochemical properties of *Galium* species. *Muş Alparslan Üniv. Fen Bilim. Derg.* **12**, 24–30 (2024).
6. Petkova, M. K., Grozeva, N. H., Tzanova, M. T. & Todorova, M. H. A review of phytochemical and pharmacological studies on *Galium verum* L., Rubiaceae. *Molecules* **30**, 1856 (2025).
7. Davis, P. H. (ed.) *Flora of Turkey and the East Aegean Islands* Vol. 7 (Edinburgh Univ. Press, 1982).
8. de la Monte, S. M. & Wands, J. R. Alzheimer's disease is type 3 diabetes—evidence reviewed. *J. Diabetes Sci. Technol.* **2**, 1101–1113 (2008).

9. Hampel, H. et al. The cholinergic system in the pathophysiology and treatment of Alzheimer's disease. *Brain* **141**, 1917–1933 (2018).

10. Dirir, A. M., Daou, M., Yousef, A. F. & Yousef, L. F. A review of alpha-glucosidase inhibitors from plants as potential candidates for the treatment of type-2 diabetes. *Phytochem. Rev.* **21**, 1049–1079 (2022).

11. Ćorković, I., Gašo-Sokač, D., Pichler, A., Šimunović, J. & Kopjar, M. Dietary polyphenols as natural inhibitors of α-amylase and α-glucosidase. *Life* **12**, 1692 (2022).

12. McMillan, J., Bester, M. J. & Apostolides, Z. In silico docking and ADMET studies on clinical targets for type 2 diabetes correlated to in vitro inhibition of pancreatic alpha-amylase and alpha-glucosidase by rutin, caffeic acid, p-coumaric acid, and vanillin. *In Silico Pharmacol.* **13** (2025). https://doi.org/10.1007/s40203-025-00324-6

13. Huang, Y., Condict, L., Richardson, S. J., Brennan, C. S. & Kasapis, S. Exploring the inhibitory mechanism of p-coumaric acid on α-amylase via multi-spectroscopic analysis, enzymatic inhibition assay and molecular docking. *Food Hydrocoll.* **139**, 108524 (2023).

14. Liu, Y. et al. A new functionality study of vanillin as the inhibitor for α-glucosidase and its inhibition kinetic mechanism. *Food Chem.* **353**, 129448 (2021).

15. Adisakwattana, S. et al. Structure–activity relationships of trans-cinnamic acid derivatives on α-glucosidase inhibition. *Bioorg. Med. Chem. Lett.* **14**, 2893–2896 (2004).

16. Lipinski, C. A., Lombardo, F., Dominy, B. W. & Feeney, P. J. Experimental and computational approaches to estimate solubility and permeability in drug discovery and development settings. *Adv. Drug Deliv. Rev.* **23**, 3–25 (1997).

17. Daina, A., Michielin, O. & Zoete, V. SwissADME: a free web tool to evaluate pharmacokinetics, drug-likeness and medicinal chemistry friendliness of small molecules. *Sci. Rep.* **7**, 42717 (2017).

18. Hollingsworth, S. A. & Dror, R. O. Molecular dynamics simulation for all. *Neuron* **99**, 1129–1143 (2018).

19. Genheden, S. & Ryde, U. The MM/PBSA and MM/GBSA methods to estimate ligand-binding affinities. *Expert Opin. Drug Discov.* **10**, 449–461 (2015).

20. Aras, A. et al. Integrated network pharmacology and in vitro/in silico evaluation of the bioactive potential of *Gundelia komagenensis* Fırat extracts. *Cytotechnology 78, 180 (2026).* https://doi.org/10.1007/s10616-026-01053-0

21. Atalar, M. N. et al. The effects of *Daucus carota* extract against PC3, PNT1a prostate cells, acetylcholinesterase, glutathione S-transferase, and α-glycosidase; an in vitro–in silico study. *J. Food Biochem.* **45**, e13975 (2021).

22. Cao, Y. Human umbilical vein endothelial cells (HUVECs) in pharmacology and toxicology: a review. *J. Appl. Toxicol.* **45**, 2512–2545 (2025).

23. Riss, T. L. & Moravec, R. A. Use of multiple assay endpoints to investigate the effects of incubation time, dose of toxin, and plating density in cell-based cytotoxicity assays. *Assay Drug Dev. Technol.* **2**, 51–62 (2004).

24. Ghasemi, M., Turnbull, T., Sebastian, S. & Kempson, I. The MTT assay: utility, limitations, pitfalls, and interpretation in bulk and single-cell analysis. *Int. J. Mol. Sci.* **22**, 12827 (2021).

25. Sabancilar, İ. et al. Potent in vitro anticancer and enzyme inhibitory activities of Anthemis fumariifolia Boiss.: LC–MS/MS fingerprinting coupled with network pharmacology and molecular simulations. *ChemistrySelect* 10, e202504480 (2025).

26. Doak, B. C., Over, B., Giordanetto, F. & Kihlberg, J. Oral druggable space beyond the rule of 5: insights from drugs and clinical candidates. Chem. Biol. 21, 1115–1142 (2014).

27. U.S. Food and Drug Administration. PRECOSE (Acarbose Tablets): Prescribing Information (FDA, 2015).

28. Pires, D. E. V., Blundell, T. L. & Ascher, D. B. pkCSM: predicting small-molecule pharmacokinetic and toxicity properties using graph-based signatures. J. Med. Chem. 58, 4066–4072 (2015).

29. Ganeshpurkar, A. & Saluja, A. K. The pharmacological potential of rutin. Saudi Pharm. J. 25, 149–164 (2017).

30. Harwood, M. et al. A critical review of the data related to the safety of quercetin and lack of evidence of in vivo toxicity, including lack of genotoxic/carcinogenic properties. Food Chem. Toxicol. 45, 2179–2205 (2007).

31. Meng, X.-Y., Zhang, H.-X., Mezei, M. & Cui, M. Molecular docking: a powerful approach for structure-based drug discovery. Curr. Comput. Aided Drug Des. 7, 146–157 (2011).

32. Pinzi, L. & Rastelli, G. Molecular docking: shifting paradigms in drug discovery. Int. J. Mol. Sci. 20, 4331 (2019).

33. Aras, A. et al. Anticancer potential, antioxidant activity, chemical content, and enzyme inhibitory properties of Inula aschersoniana Janka, supported by an integrated network pharmacology study. Cytotechnology 78 (2026). https://doi.org/10.1007/s10616-026-00955-3

34. Cheung, J. et al. Structures of human acetylcholinesterase in complex with pharmacologically important ligands. J. Med. Chem. 55, 10282–10286 (2012).

35. Hopkins, A. L., Groom, C. R. & Alex, A. Ligand efficiency: a useful metric for lead selection. Drug Discov. Today 9, 430–431 (2004).

36. Hou, T., Wang, J., Li, Y. & Wang, W. Assessing the performance of the MM/PBSA and MM/GBSA methods. 1. The accuracy of binding free energy calculations based on molecular dynamics simulations. J. Chem. Inf. Model. 51, 69–82 (2011).

37. Atalar, M. N. et al. Phytochemical analysis and biological activity of *Corchorus olitorius* L.: quantitative analysis of bioactive compounds by LC–MS/MS, antibacterial, enzyme inhibition, and cytotoxic activities. *Eur. J. Integr. Med.* **62**, 102290 (2023).

38. Re, R. et al. Antioxidant activity applying an improved ABTS radical cation decolorization assay. *Free Radic. Biol. Med.* **26**, 1231–1237 (1999).

39. Erel, O. A novel automated direct measurement method for total antioxidant capacity using a new generation, more stable ABTS radical cation. *Clin. Biochem.* **37**, 277–285 (2004).

40. Oyaizu, M. Studies on products of browning reaction. Antioxidative activities of products of browning reaction prepared from glucosamine. Jpn. J. Nutr. Diet. 44, 307–315 (1986).

41. Bursal, E., Aras, A., Dogru, M. & Kılıç, Ö. Phenolic content, antioxidant potentials of *Saponaria prostrata* endemic plant. *Int. J. Life Sci. Biotechnol.* **5**, 1–8 (2022).

42. Işık, M. et al. Changes in the anti-oxidant system in adult epilepsy patients receiving anti-epileptic drugs. *Arch. Physiol. Biochem.* **121**, 97–102 (2015).

43. Ellman, G. L., Courtney, K. D., Andres, V. & Featherstone, R. M. A new and rapid colorimetric determination of acetylcholinesterase activity. *Biochem. Pharmacol.* **7**, 88–95 (1961).

44. Xiao, Z., Storms, R. & Tsang, A. A quantitative starch–iodine method for measuring alpha-amylase and glucoamylase activities. *Anal. Biochem.* **351**, 146–148 (2006).

45. Tao, Y., Zhang, Y., Cheng, Y. & Wang, Y. Rapid screening and identification of α-glucosidase inhibitors from mulberry leaves using enzyme-immobilized magnetic beads coupled with HPLC/MS and NMR. *Biomed. Chromatogr.* **27**, 148–155 (2013).

46. O'Boyle, N. M. et al. Open Babel: an open chemical toolbox. *J. Cheminform.* **3**, 33 (2011).

47. Landrum, G. et al. RDKit: open-source cheminformatics. *Zenodo* https://doi.org/10.5281/zenodo.591637 (2024).

48. Berman, H. M. et al. The Protein Data Bank. *Nucleic Acids Res.* **28**, 235–242 (2000).

49. Trott, O. & Olson, A. J. AutoDock Vina: improving the speed and accuracy of docking with a new scoring function, efficient optimization, and multithreading. *J. Comput. Chem.* **31**, 455–461 (2010).

50. Eberhardt, J., Santos-Martins, D., Tillack, A. F. & Forli, S. AutoDock Vina 1.2.0: new docking methods, expanded force field, and Python bindings. *J. Chem. Inf. Model.* **61**, 3891–3898 (2021).

51. Dassault Systèmes BIOVIA. *Discovery Studio Visualizer* v.2019 (Dassault Systèmes, 2019).

52. Schrödinger, LLC. *The PyMOL Molecular Graphics System* v.2.5 (Schrödinger, LLC).

53. Abraham, M. J. et al. GROMACS: high performance molecular simulations through multi-level parallelism from laptops to supercomputers. *SoftwareX* **1–2**, 19–25 (2015).

54. Jo, S., Kim, T., Iyer, V. G. & Im, W. CHARMM-GUI: a web-based graphical user interface for CHARMM. *J. Comput. Chem.* **29**, 1859–1865 (2008).

55. Huang, J. et al. CHARMM36m: an improved force field for folded and intrinsically disordered proteins. *Nat. Methods* **14**, 71–73 (2017).

56. Vanommeslaeghe, K. et al. CHARMM general force field: a force field for drug-like molecules compatible with the CHARMM all-atom additive biological force fields. *J. Comput. Chem.* **31**, 671–690 (2010).

57. Jorgensen, W. L., Chandrasekhar, J., Madura, J. D., Impey, R. W. & Klein, M. L. Comparison of simple potential functions for simulating liquid water. *J. Chem. Phys.* **79**, 926–935 (1983).

58. Bussi, G., Donadio, D. & Parrinello, M. Canonical sampling through velocity rescaling. *J. Chem. Phys.* **126**, 014101 (2007).

59. Bernetti, M. & Bussi, G. Pressure control using stochastic cell rescaling. *J. Chem. Phys.* **153**, 114107 (2020).

60. Parrinello, M. & Rahman, A. Polymorphic transitions in single crystals: a new molecular dynamics method. *J. Appl. Phys.* **52**, 7182–7190 (1981).

61. Hess, B., Bekker, H., Berendsen, H. J. C. & Fraaije, J. G. E. M. LINCS: a linear constraint solver for molecular simulations. *J. Comput. Chem.* **18**, 1463–1472 (1997).

62. Darden, T., York, D. & Pedersen, L. Particle mesh Ewald: an N·log(N) method for Ewald sums in large systems. *J. Chem. Phys.* **98**, 10089–10092 (1993).

63. Valdés-Tresanco, M. S., Valdés-Tresanco, M. E., Valiente, P. A. & Moreno, E. gmx_MMPBSA: a new tool to perform end-state free energy calculations with GROMACS. *J. Chem. Theory Comput.* **17**, 6281–6291 (2021).

64. Miller, B. R. et al. MMPBSA.py: an efficient program for end-state free energy calculations. *J. Chem. Theory Comput.* **8**, 3314–3321 (2012).

65. Onufriev, A., Bashford, D. & Case, D. A. Exploring protein native states and large-scale conformational changes with a modified generalized Born model. *Proteins* **55**, 383–394 (2004).

Acknowledgements

This research received no specific grant from any funding agency.

Author contributions

Conceptualization, A.A., M.D., İ.S., M.Y.; methodology, A.A., M.Y., A.B., İ.S., E.O., F.T.; investigation, A.A., A.B., M.D., Ö.K.; in silico analyses (molecular docking, molecular dynamics, and MM/GBSA), A.B.; data curation and formal analysis, A.A., M.Y., İ.S., M.D.; writing—original draft, A.A., M.Y., İ.S., A.B.; writing—review and editing, A.A., İ.S., M.Y.; supervision, A.A. All authors reviewed and approved the final version of the manuscript.

Funding

This research received no specific grant from any funding agency.

Competing interests

The authors declare no competing interests.